arXiv:hep-ph/0011044v3 4 Apr 2001

A Gaussian Sum-Rules Analysis of Scalar Glueballs

D. Harnett, T.G. Steele*
Department of Physics and Engineering Physics
University of Saskatchewan
Saskatoon, Saskatchewan, S7N 5E2
Canada

February 1, 2008

Abstract

Although marginally more complicated than the traditional Laplace sum-rules, Gaussian sum-rules have the advantage of being able to probe excited and ground states with similar sensitivity. Gaussian sum-rule analysis techniques are applied to the problematic scalar glueball channel to determine masses, widths and relative resonance strengths of low-lying scalar glueball states contributing to the hadronic spectral function. A feature of our analysis is the inclusion of instanton contributions to the scalar gluonic correlation function. Compared with the next-to-leading Gaussian sum-rule, the analysis of the lowest-weighted sum-rule (which contains a large scale-independent contribution from the low energy theorem) is shown to be unreliable because of instability under QCD uncertainties. However, the presence of instanton effects leads to approximately consistent mass scales in the lowest weighted and next-lowest weighted sum-rules. The analysis of the next-to-leading sum-rule demonstrates that a single narrow resonance model does *not* provide an adequate description of the hadronic spectral function. Consequently, we consider a wide variety of phenomenological models which distribute resonance strength over a broad region—some of which lead to excellent agreement between the theoretical prediction and phenomenological models. Including QCD uncertainties, our results indicate that the hadronic contributions to the spectral function stem from a pair of resonances with masses in the range 0.8–1.6 GeV, with the lighter of the two potentially having a large width.

1 Introduction

Mass predictions for scalar (0^{++}) glueballs extracted from QCD sum-rules have been problematic mainly due to discrepancies between analyses which are sensitive to the low-energy theorem for gluonic correlation functions and those which are insensitive to this quantity [1, 2, 3, 4, 5, 6]. Such a discrepancy would be indicative of two widely-separated states, a result which has already been seen to occur in explicit two-resonance analyses of Laplace sum-rules even in the absence of mixing with quark scalar resonances [3, 4]. However, there exists substantial evidence that these discrepancies are resolved by the inclusion of instanton [7] effects in the Laplace sum-rules for scalar glueballs [5, 6].

Recently, techniques for using Gaussian sum-rules [8] to predict hadronic properties have been developed [9]. In particular, these methods concentrate on normalized Gaussian sum-rules which are independent of the finite-energy sum-rule constraint which is central to the original heat-evolution studies [8] of the Gaussian sum-rules. Advantages of this approach compared with Laplace sum-rules include enhanced sensitivity to the hadronic spectral function over a wide range of energy. In this paper, these techniques are employed and generalized in an effort to obtain resonance parameter predictions for scalar gluonium. Furthermore, the formulation of these sum-rules is extended

---

*email: Tom.Steele@usask.ca

to include Gaussian kernels weighted by integer powers,

$$\frac{1}{\sqrt{4\pi\tau}}\int\limits_{t_0}^{\infty} t^k \exp\left[-\frac{(t-\hat{s})^2}{4\tau}\right]\frac{1}{\pi}\rho(t)\mathrm{d}t \quad , \quad k\geq -1 \tag{1}$$

where $\rho(t)$ is a hadronic spectral function with physical threshold t_0. Similar to the Laplace sum-rules, the low-energy theorem (LET) [10] (see (8) below) for scalar gluonic currents enters *only* the $k=-1$ Gaussian sum-rule, and instanton contributions to the correlation function serve to mitigate the discrepancy between the $k=-1$ and $k>-1$ sum-rules. However, theoretical uncertainties associated with the instanton and LET parameters are shown to be overwhelming in the $k=-1$ sum-rule, rendering it unsuitable for phenomenological analysis. Thus the $k=0$ Gaussian sum-rule is the focus of our detailed predictions for scalar glueballs, including an estimate of theoretical uncertainties.

We show that the Gaussian sum-rules of scalar gluonic currents contain signatures that the hadronic spectral function is distributed over a broad energy range, (0.8–1.6) GeV including QCD uncertainties, and that this distribution most likely consists of two separate resonances. Since these sum-rules probe the gluonic content of hadronic states, they are sensitive to the glueball component of the observed scalar mesons which in general could be glueball-quark meson mixtures. Thus our results are relevant to the interpretation of the scalar isoscalar resonances in this region: the $f_0(400\text{–}1200)$, $f_0(980)$, $f_0(1370)$, $f_0(1500)$, and $f_0(1710)$ [11].

In the next section, Gaussian sum-rules for scalar gluonic currents are developed. In Section 3, we develop analysis techniques and employ them to analyze the Gaussian sum-rules using a variety of phenomenological models. The results of this phenomenological analysis, including theoretical uncertainties, are consolidated in Section 4, and a summary of our results is contained in Section 5.

2 Scalar Glueball Gaussian Sum-Rules

The most important quantity in any sum-rules approach to determining hadron properties is the correlation function for the particular channel under inspection:

$$\Pi(Q^2)=\mathrm{i}\int \mathrm{d}^4x\, \mathrm{e}^{\mathrm{i}q\cdot x}\langle\Omega|T\{J(x),J(0)\}|\Omega\rangle \quad , \quad Q^2=-q^2 \tag{2}$$

where $|\Omega\rangle$ is the QCD vacuum state, T is the time-ordering operator, and $J(x)$ is that current which corresponds to the quantum numbers of interest. In this paper, we wish to focus on scalar glueballs and so we choose the following current:

$$J=-\frac{\pi^2}{\alpha\beta_0}\beta(\alpha)G^a{}_{\mu\nu}G^{a\mu\nu} \tag{3}$$

which is renormalization-group invariant in the chiral limit of n_f massless quarks. The gluon field strength tensor $G^a{}_{\mu\nu}$ is defined by

$$G^a{}_{\mu\nu}=\partial_\mu A^a_\nu-\partial_\nu A^a_\mu+gf^{abc}A^b_\mu A^c_\nu \tag{4}$$

and $\beta(\alpha)$ is the QCD beta function describing the momentum scale dependence of the strong coupling parameter α

$$\beta\left(\alpha\right)=\nu^2\frac{d}{d\nu^2}\left(\frac{\alpha(\nu)}{\pi}\right)=-\beta_0\left(\frac{\alpha}{\pi}\right)^2-\beta_1\left(\frac{\alpha}{\pi}\right)^3+\dots \tag{5}$$

$$\beta_0=\frac{11}{4}-\frac{1}{6}n_f \quad , \quad \beta_1=\frac{51}{8}-\frac{19}{24}n_f \quad , \quad \dots \quad . \tag{6}$$

From the asymptotic form and assumed analytic properties of (2) follows a dispersion relation with three subtraction constants

$$\Pi(Q^2)-\Pi(0)-Q^2\Pi'(0)-\frac{1}{2}Q^4\Pi''(0)=-\frac{Q^6}{\pi}\int_{t_0}^{\infty}\frac{\rho(t)}{t^3(t+Q^2)}\mathrm{d}t \quad , \quad Q^2>0 \tag{7}$$

where $\rho(t)$ is the hadronic spectral function[1] with physical threshold t_0. The spectral function $\rho(t)$ is related to a physical process and is thus determined phenomenologically. In contrast, $\Pi(Q^2)$ is calculated theoretically from QCD, and the constant $\Pi(0)$ follows from the low-energy theorem [10]

$$\Pi(0) \equiv \lim_{Q^2 \to 0} \Pi(Q^2) = \frac{8\pi}{\beta_0} \langle J \rangle \quad . \tag{8}$$

For these reasons, we shall refer to the left-hand side of (7) as the theoretical side and the right-hand side as the phenomenological side. In this regard, eqn. (7) serves to relate theory to phenomenology, and, in principle, could be used to predict the properties of hadrons from QCD.

However, as it stands, eqn. (7) is not actually that well-suited to this task. For instance, although the constant $\Pi(0)$ is determined by the low-energy theorem (8), the constants $\Pi'(0)$ and $\Pi''(0)$ are not. Further, the theoretical calculation of $\Pi(Q^2)$ contains a field theoretical divergence proportional to Q^4. In addition, from a phenomenological perspective, the integral on the right-hand side of (7) is far too sensitive to the high energy behaviour of $\rho(t)$ to effectively probe low-lying resonances.

To circumvent these shortcomings, we consider the one-parameter family of Gaussian sum-rules[2]

$$G_k(\hat{s}, \tau) \equiv \sqrt{\frac{\tau}{\pi}} \mathcal{B} \left\{ \frac{(\hat{s} + \mathrm{i}\Delta)^k \Pi(-\hat{s} - \mathrm{i}\Delta) - (\hat{s} - \mathrm{i}\Delta)^k \Pi(-\hat{s} + \mathrm{i}\Delta)}{\mathrm{i}\Delta} \right\} \quad , \quad k \geq -1 \tag{9}$$

with the Borel transform $\mathcal{B}$ defined by

$$\mathcal{B} \equiv \lim_{\substack{N, \Delta^2 \to \infty \\ \Delta^2/N \equiv 4\tau}} \frac{(-\Delta^2)^N}{\Gamma(N)} \left(\frac{\mathrm{d}}{\mathrm{d}\Delta^2} \right)^N \quad . \tag{10}$$

Applying definition (9) to both sides of (7) alleviates the difficulties surrounding (7): the infinite number of derivatives in (10) annihilate the unwanted low-energy constants and the field theoretical divergence contained in $\Pi(Q^2)$. Furthermore, as we shall see, a key feature of the resulting sum-rules is the introduction of a Gaussian weight factor to the integrand on the phenomenological side of (7). This serves to suppress contributions from $\rho(t)$ away from the Gaussian peak—a desirable situation considering that we wish to extract information concerning low-lying resonances.

Let us first consider (9) as applied to the theoretical side of (7). As noted previously, the low-energy constants $\Pi'(0)$ and $\Pi''(0)$ are annihilated by the Borel transform; however, the constant $\Pi(0)$ does produce a contribution unique to the case $k = -1$. Using the following identity:

$$\mathcal{B} \left[\frac{(\Delta^2)^n}{\Delta^2 + a} \right] = \frac{1}{4\tau} (-a)^n \exp\left(\frac{-a}{4\tau} \right) \ \text{for } n \geq 0 \quad , \tag{11}$$

it is trivial to show that the contribution to the theoretical side of the Gaussian sum-rules devolving from the low-energy constant is given by

$$\frac{1}{\sqrt{4\pi\tau}} \exp\left(\frac{-\hat{s}^2}{4\tau} \right) \Pi(0) \quad . \tag{12}$$

To proceed further, however, we must settle on a specific form for the scalar glueball correlator $\Pi(Q^2)$. We choose to partition the correlator into the following sum of qualitatively distinct terms:

$$\Pi^{\mathrm{QCD}}(Q^2) = \Pi^{\mathrm{pert}}(Q^2) + \Pi^{\mathrm{cond}}(Q^2) + \Pi^{\mathrm{inst}}(Q^2) \quad , \tag{13}$$

where the superscript *QCD* signifies that (13) is a theoretical approximation to the true correlator. The first two terms in (13) devolve from the operator product expansion of the current (3). The quantity $\Pi^{\mathrm{pert}}(Q^2)$ is the contribution from ordinary perturbation theory whereas $\Pi^{\rm cond}(Q^2)$ is the result of nonzero vacuum expectation values of local gluonic operators (condensates). For three colours and three flavours of massless quarks ($n_{\rm f}=3$), $\Pi^{\rm pert}(Q^2)$ is given at three-loop order by [12]

---

[1] In the literature, $\rho(t)$ is often denoted by $\mathrm{Im}\Pi(t)$.

[2] This definition is a natural generalization of that given in [8]. To recover the original Gaussian sum-rule, we simply let $k = 0$ in (9).

$$\Pi^{\rm pert}(Q^2) = Q^4 \log\left(\frac{Q^2}{\nu^2}\right)\left[a_0 + a_1\log\left(\frac{Q^2}{\nu^2}\right) + a_2\log^2\left(\frac{Q^2}{\nu^2}\right)\right] \tag{14}$$

$$a_0 = -2\left(\frac{\alpha}{\pi}\right)^2\left[1+\frac{659}{36}\frac{\alpha}{\pi}+247.480\left(\frac{\alpha}{\pi}\right)^2\right]\ ,\quad a_1 = 2\left(\frac{\alpha}{\pi}\right)^3\left[\frac{9}{4}+65.781\frac{\alpha}{\pi}\right]\ ,\quad a_2=-10.1250\left(\frac{\alpha}{\pi}\right)^4 \tag{15}$$

where we have omitted the aforementioned field theoretical divergence as this term is annihilated by the Borel operator (10). Incorporating into $\Pi^{\rm cond}(Q^2)$ next-to-leading order [13] contributions[3] from the dimension four gluon condensate $\langle J\rangle$ and leading order [1] contributions from gluonic condensates of dimension six and eight

$$\langle\mathcal{O}_6\rangle = \left\langle g f_{abc} G^a_{\mu\nu} G^b_{\nu\rho} G^c_{\rho\mu}\right\rangle \tag{16}$$

$$\langle\mathcal{O}_8\rangle = 14\left\langle\left(\alpha f_{abc} G^a_{\mu\rho} G^b_{\nu\rho}\right)^2\right\rangle - \left\langle\left(\alpha f_{abc} G^a_{\mu\nu} G^b_{\rho\lambda}\right)^2\right\rangle \tag{17}$$

yields

$$\Pi^{\rm cond}(Q^2) = \left[b_0 + b_1\log\left(\frac{Q^2}{\nu^2}\right)\right]\langle J\rangle + \frac{c_0}{Q^2}\langle\mathcal{O}_6\rangle + \frac{d_0}{Q^4}\langle\mathcal{O}_8\rangle \tag{18}$$

$$b_0 = 4\pi\frac{\alpha}{\pi}\left[1+\frac{175}{36}\frac{\alpha}{\pi}\right]\ ,\quad b_1 = -9\pi\left(\frac{\alpha}{\pi}\right)^2\ ,\quad c_0 = 8\pi^2\left(\frac{\alpha}{\pi}\right)^2\ ,\quad d_0 = 8\pi^2\frac{\alpha}{\pi}\quad . \tag{19}$$

The final term on the right-hand side of (13) is a contribution arising from direct instanton effects. Note that in decoupling this term from perturbation theory and the condensate contributions, we have tacitly assumed that interference between classical and quantum fields is small. Further, we also assume that the dominant contribution to $\Pi^{\rm inst}(Q^2)$ comes from BPST single instanton and anti-instanton solutions [7] and that multi-instanton effects are negligible [14]. With these provisions, we have [1, 5, 6, 15]

$$\Pi^{\rm inst}\left(Q^2\right) = 32\pi^2 Q^4 \int \rho^4\left[K_2\left(\rho\sqrt{Q^2}\right)\right]^2 {\rm d}n(\rho)\quad , \tag{20}$$

where $K_2(x)$ is the modified Bessel function of the second kind of order two (*c.f.* [16]), ρ is the instanton radius, and $n(\rho)$ is the instanton density function.

Before substituting (13) into (9), it is convenient to first simplify (9) by employing a particularly useful identity relating the Borel transform (10) to the inverse Laplace transform [8]

$$\mathcal{B}[f(\Delta^2)] = \frac{1}{4\tau}\mathcal{L}^{-1}[f(\Delta^2)] \tag{21}$$

where, in our notation,

$$\mathcal{L}^{-1}[f(\Delta^2)] = \frac{1}{2\pi i}\int_{a-{\rm i}\infty}^{a+{\rm i}\infty} f(\Delta^2)\exp\left(\frac{\Delta^2}{4\tau}\right){\rm d}\Delta^2 \tag{22}$$

with a chosen such that all singularities of f lie to the left of a in the complex Δ^2-plane. (Note, there is no loss of generality in assuming that $a>0$.) Rewriting (9) using (21) gives

$$G_k(\hat{s},\tau) = \frac{1}{4\sqrt{\pi\tau}}\frac{1}{2\pi i}\left\{\int_{a-i\infty}^{a+i\infty}\frac{(\hat{s}+{\rm i}\Delta)^k\Pi(-\hat{s}-{\rm i}\Delta)}{{\rm i}\Delta}\exp\left(\frac{\Delta^2}{4\tau}\right){\rm d}\Delta^2\right.$$
$$\left. - \int_{a-i\infty}^{a+i\infty}\frac{(\hat{s}-{\rm i}\Delta)^k\Pi(-\hat{s}+{\rm i}\Delta)}{{\rm i}\Delta}\exp\left(\frac{\Delta^2}{4\tau}\right){\rm d}\Delta^2\right\}\quad . \tag{23}$$

---

[3] The calculation of next-to-leading contributions in [13] have been extended non-trivially to $n_f=3$ from $n_f=0$, and the operator basis has been changed from $\langle\alpha G^2\rangle$ to $\langle J\rangle$.

If in the first integral above, we make the substitution $w = -\hat{s} - \mathrm{i}\Delta$ and in the second, we make the substitution $w = -\hat{s} + \mathrm{i}\Delta$, then (23) reduces to

$$G_k(\hat{s},\tau) = \frac{1}{4\sqrt{\pi\tau}}\frac{1}{2\pi i}\left\{2\int_{\Gamma_1}(-w)^k \exp\left[\frac{-(\hat{s}+w)^2}{4\tau}\right]\Pi(w)\mathrm{d}w + 2\int_{\Gamma_2}(-w)^k \exp\left[\frac{-(\hat{s}+w)^2}{4\tau}\right]\Pi(w)\mathrm{d}w\right\} \tag{24}$$

$$= \frac{1}{\sqrt{4\pi\tau}}\frac{1}{2\pi i}\int_{\Gamma_1+\Gamma_2}(-w)^k \exp\left[\frac{-(\hat{s}+w)^2}{4\tau}\right]\Pi(w)\mathrm{d}w \tag{25}$$

where Γ_1 and Γ_2 are two parabolas (depicted in Figure 1) in the complex w-plane defined by

$$\Gamma_1 = -\hat{s} - \mathrm{i}(a^2+x^2)^{1/4}\exp\left[\frac{\mathrm{i}}{2}\mathrm{Arctan}\left(\frac{x}{a}\right)\right] \tag{26}$$

$$\Gamma_1 = -\hat{s} + \mathrm{i}(a^2+x^2)^{1/4}\exp\left[\frac{\mathrm{i}}{2}\mathrm{Arctan}\left(\frac{x}{a}\right)\right] \tag{27}$$

for all $x \in \mathbb{R}$.

Now, we must substitute (13) into (25) and calculate the resulting complicated integral. Towards this end, it is advantageous to consider the closed contour $C(R)$ depicted in Figure 2. Our expression for the correlator (13) is analytic in the complex $w \equiv Q^2$-plane except for a branch cut along the negative real semi-axis originating from a branch point located at the origin. Consequently,

$$0 = \frac{1}{2\pi i}\frac{1}{\sqrt{4\pi\tau}}\oint_{C(R)}(-w)^k \exp\left[\frac{-(\hat{s}+w)^2}{4\tau}\right]\Pi^{\mathrm{QCD}}(w)\mathrm{d}w \tag{28}$$

$$= \frac{1}{2\pi i}\frac{1}{\sqrt{4\pi\tau}}\left\{\int_{\tilde{\Gamma}_1(R)+\tilde{\Gamma}_2(R)} + \int_{\Gamma_c+\Gamma_\epsilon} + \int_{\Gamma_3+\Gamma_4+\Gamma_5}\right\}(-w)^k \exp\left[\frac{-(\hat{s}+w)^2}{4\tau}\right]\Pi^{\mathrm{QCD}}(w)\mathrm{d}w \tag{29}$$

where $\tilde{\Gamma}_1(R)$ and $\tilde{\Gamma}_2(R)$ are respectively those portions of the contours Γ_1 and Γ_2 (see (26) and (27)) lying in the interior of a circle of radius R centered at $-\hat{s}$. For large R, the integral over $\Gamma_3+\Gamma_4+\Gamma_5$ approaches zero and the contours $\tilde{\Gamma}_1(R)$ and $\tilde{\Gamma}_2(R)$ approach Γ_1 and Γ_2. Therefore, by rearranging (29), recalling (25), and taking appropriate limits, we get

$$G_k^{\mathrm{QCD}}(\hat{s},\tau) = -\frac{1}{2\pi\mathrm{i}}\frac{1}{\sqrt{4\pi\tau}}\lim_{\substack{R\to\infty\\ \epsilon\to 0}}\int_{\Gamma_c+\Gamma_\epsilon}(-w)^k \exp\left[\frac{-(\hat{s}+w)^2}{4\tau}\right]\Pi^{\mathrm{QCD}}(w)\mathrm{d}w \tag{30}$$

$$= \frac{1}{2\pi\mathrm{i}}\frac{(-1)^{k+1}}{\sqrt{4\pi\tau}}\lim_{\epsilon\to 0}\int_{\Gamma_\epsilon} w^k \exp\left[\frac{-(\hat{s}+w)^2}{4\tau}\right]\Pi^{\mathrm{QCD}}(w)\mathrm{d}w + \frac{1}{\sqrt{4\pi\tau}}\lim_{\epsilon\to 0}\int_\epsilon^\infty t^k \exp\left[\frac{-(\hat{s}-t)^2}{4\tau}\right]\frac{1}{\pi}\mathrm{Im}\Pi^{\mathrm{QCD}}(t)\mathrm{d}t \quad , \tag{31}$$

where

$$\mathrm{Im}\Pi^{\mathrm{QCD}}(t) \equiv \lim_{\delta\to 0^+}\left[\frac{\Pi^{\mathrm{QCD}}(-t-\mathrm{i}\delta) - \Pi^{\mathrm{QCD}}(-t+\mathrm{i}\delta)}{2\mathrm{i}}\right] \quad . \tag{32}$$

Eqn. (31) is our final expression for the contribution to the k-th Gaussian sum-rule of scalar gluonium stemming from the correlator (13). Later in this section, however, we do evaluate (31) for the specific cases $k = -1, 0$ (see (41) and (42)).

We must now consider the phenomenological contribution to the Gaussian sum-rules. Substituting the right-hand side of (7) into (9) and again making use of the identity (11), it is simple to show that

$$G_k^{\mathrm{phen}}(\hat{s},\tau) = \frac{1}{\sqrt{4\pi\tau}}\int_{t_0}^\infty t^k \exp\left[\frac{-(\hat{s}-t)^2}{4\tau}\right]\frac{1}{\pi}\rho(t)\mathrm{d}t \quad . \tag{33}$$

In sum-rules analyses, it is customary to approximate the spectral function $\rho(t)$ using a "resonance(s) + continuum" ansatz. In this model, hadronic physics is (locally) dual to QCD above the continuum threshold s_0, and so we write

$$\rho(t) = \rho^{\rm had}(t) + \theta\left(t - s_0\right) {\rm Im}\Pi^{\rm QCD}(t) \tag{34}$$

where $\theta(t)$ is the Heaviside step function. (We shall have much more to say concerning $\rho^{\rm had}(t)$ in Section 3.)

Substituting (34) into (33) and comparing the result to the theoretical expression (31) shows us that the continuum contribution

$$G_k^{\rm cont}(\hat{s},\tau,s_0) = \frac{1}{\sqrt{4\pi\tau}}\int_{s_0}^{\infty} t^k \exp\left[\frac{-(\hat{s}-t)^2}{4\tau}\right]\frac{1}{\pi}{\rm Im}\Pi^{\rm QCD}(t){\rm d}t \tag{35}$$

is common to both; therefore, we define

$$G_k^{\rm QCD}(\hat{s},\tau,s_0) \equiv G_k^{\rm QCD}(\hat{s},\tau) - G_k^{\rm cont}(\hat{s},\tau,s_0) \tag{36}$$

$$G_k^{\rm had}(\hat{s},\tau) \equiv G_k^{\rm phen}(\hat{s},\tau) - G_k^{\rm cont}(\hat{s},\tau,s_0) \tag{37}$$

and write (recall the low-energy contribution (12) unique to the $k = -1$ sum-rule)

$$G_{-1}^{\rm QCD}(\hat{s},\tau,s_0) + \frac{1}{\sqrt{4\pi\tau}}\exp\left(\frac{-\hat{s}^2}{4\tau}\right)\Pi(0) = G_{-1}^{\rm had}(\hat{s},\tau) \tag{38}$$

$$G_k^{\rm QCD}(\hat{s},\tau,s_0) = G_k^{\rm had}(\hat{s},\tau) \quad , \quad k \geq 0 \tag{39}$$

with

$$G_k^{\rm had}(\hat{s},\tau) = \frac{1}{\sqrt{4\pi\tau}}\int_{t_0}^{\infty} t^k \exp\left[\frac{-(\hat{s}-t)^2}{4\tau}\right]\frac{1}{\pi}\rho^{\rm had}(t){\rm d}t \quad , \quad k \geq -1 \quad . \tag{40}$$

We note that (38–40) have meaning for $\hat{s} < 0$ since this simply represents a Gaussian kernel whose peak lies outside the $t > 0$ physical region, and hence only the Gaussian tail extends into the physical region. As will later be shown, the QCD results scale with τ through the renormalization-group equation, and hence QCD also presents no obstacles to considering $\hat{s} < 0$. Indeed, the seminal work [8] on Gaussian sum-rules considered symmetric and antisymmetric combinations $U^{\pm}\left(\hat{s},\tau\right) = G\left(\hat{s},\tau\right) \pm G\left(-\hat{s},\tau\right)$ which implicitly employs Gaussian sum-rules with negative $\hat{s}$.

In this paper, we focus exclusively on the $k = 0, -1$ Gaussian sum-rules. Substituting (13) into (36) and recalling (31) gives[4] (for details on simplifying the relevant integrals in (31), see [6, 9])

$$\begin{aligned}
G_{-1}^{\rm QCD}(\hat{s},\tau,s_0) = &-\frac{1}{\sqrt{4\pi\tau}}\int_0^{s_0} t\exp\left[\frac{-(\hat{s}-t)^2}{4\tau}\right]\left[(a_0-\pi^2 a_2) + 2a_1\log\left(\frac{t}{\nu^2}\right) + 3a_2\log^2\left(\frac{t}{\nu^2}\right)\right]{\rm d}t\\
&+\frac{1}{\sqrt{4\pi\tau}}\exp\left(\frac{-\hat{s}^2}{4\tau}\right)\left[-b_0\langle J\rangle + \frac{c_0\hat{s}}{2\tau}\left\langle\mathcal{O}_6\right\rangle - \frac{d_0}{4\tau}\left(\frac{\hat{s}^2}{2\tau}-1\right)\left\langle\mathcal{O}_8\right\rangle\right]\\
&-\frac{16\pi^3}{\sqrt{4\pi\tau}}\int {\rm d}n(\rho)\rho^4\int_0^{s_0} t\exp\left[\frac{-(\hat{s}-t)^2}{4\tau}\right] J_2\left(\rho\sqrt{t}\right)Y_2\left(\rho\sqrt{t}\right){\rm d}t\\
&-\frac{128\pi^2}{\sqrt{4\pi\tau}}\exp\left(\frac{-\hat{s}^2}{4\tau}\right)\int {\rm d}n(\rho)
\end{aligned} \tag{41}$$

$$\begin{aligned}
G_{0}^{\rm QCD}(\hat{s},\tau,s_0) = &-\frac{1}{\sqrt{4\pi\tau}}\int_0^{s_0} t^2\exp\left[\frac{-(\hat{s}-t)^2}{4\tau}\right]\left[(a_0-\pi^2 a_2) + 2a_1\log\left(\frac{t}{\nu^2}\right) + 3a_2\log^2\left(\frac{t}{\nu^2}\right)\right]{\rm d}t\\
&-\frac{1}{\sqrt{4\pi\tau}}b_1\langle J\rangle\int_0^{s_0}\exp\left[\frac{-(\hat{s}-t)^2}{4\tau}\right]{\rm d}t + \frac{1}{\sqrt{4\pi\tau}}\exp\left(\frac{-\hat{s}^2}{4\tau}\right)\left[c_0\left\langle\mathcal{O}_6\right\rangle - \frac{d_0\hat{s}}{2\tau}\left\langle\mathcal{O}_8\right\rangle\right]\\
&-\frac{16\pi^3}{\sqrt{4\pi\tau}}\int {\rm d}n(\rho)\rho^4\int_0^{s_0} t^2\exp\left[\frac{-(\hat{s}-t)^2}{4\tau}\right] J_2\left(\rho\sqrt{t}\right)Y_2\left(\rho\sqrt{t}\right){\rm d}t
\end{aligned} \tag{42}$$

---

[4] The given result is valid to leading order in the condensates.

where $J_2(x)$ and $Y_2(x)$ are Bessel functions of order two of the first and second kind respectively (*c.f.* [16]). Renormalization-group improvements [8, 17] of (41) and (42) amount to replacing the strong coupling constant α (contained in the coefficients (15) and (19)) by the running coupling $\alpha(\nu^2)$ at the renormalization scale $\nu^2 = \sqrt{\tau}$. At three loop order with $n_{\rm f} = 3$ in the $\overline{\rm MS}$ renormalization scheme, we have [11]

$$\frac{\alpha(\nu^2)}{\pi} = \frac{1}{\beta_0 L} - \frac{\bar\beta_1 \log L}{\left(\beta_0 L\right)^2} + \frac{1}{\left(\beta_0 L\right)^3}\left[\bar\beta_1^2\left(\log^2 L - \log L - 1\right) + \bar\beta_2\right] \tag{43}$$

$$L = \log\left(\frac{\nu^2}{\Lambda^2}\right) \quad , \quad \bar\beta_i = \frac{\beta_i}{\beta_0} \quad , \quad \beta_0 = \frac{9}{4} \quad , \quad \beta_1 = 4 \quad , \quad \beta_2 = \frac{3863}{384} \tag{44}$$

with $\Lambda_{\overline{MS}} \approx 300\,{\rm MeV}$ for three active flavours, consistent with current estimates of $\alpha(M_\tau)$ [11] [5] and matching conditions through the charm threshold [19].

The normalization of the Gaussian sum-rules is related to the finite-energy sum-rules (FESRs) [20] as can be seen by integrating (38) and (39) with respect to $\hat s$ to obtain

$$\int\limits_{-\infty}^{\infty} G_{-1}^{\rm QCD}(\hat s, \tau, s_0){\rm d}\hat s + \Pi(0) = \frac{1}{\pi}\int\limits_{t_0}^{\infty} \frac{1}{t}\rho^{\rm had}(t){\rm d}t \tag{45}$$

$$\int\limits_{-\infty}^{\infty} G_{k}^{\rm QCD}(\hat s, \tau, s_0){\rm d}\hat s = \frac{1}{\pi}\int\limits_{t_0}^{\infty} t^k\rho^{\rm had}(t){\rm d}t \quad , \quad k \geq 0. \tag{46}$$

We recognize the quantities on the right-hand sides of (45) and (46) from the definition of the (FESRs)

$$F_k\left(s_0\right) = \frac{1}{\pi}\int\limits_{t_0}^{\infty} {\rm d}t\, t^k \rho^{\rm had}(t) \quad , \tag{47}$$

where F_k represents a QCD prediction. Thus we see that the overall normalization of $G_k^{\rm QCD}$ (or $G_{-1}^{\rm QCD} + \Pi(0)$) is constrained by the finite-energy sum-rules.

This result is not surprising in light of the seminal work on Gaussian sum-rules which established the significance of the FESR constraint by considering the evolution of the Gaussian sum-rules through the diffusion equation [8]. It was found that this "heat-evolution" of the resonance plus continuum model would only reproduce the QCD prediction in the asymptotic regime if the continuum s_0 was constrained by the lowest FESR. Hence, the normalization of the Gaussian sum-rules, which is constrained by the FESR, should be removed by defining normalized (unit-area) Gaussian sum-rules

$$N_{-1}^{\rm QCD}(\hat s, \tau, s_0) \equiv \frac{G_{-1}^{\rm QCD}(\hat s, \tau, s_0) + \frac{1}{\sqrt{4\pi\tau}}\exp\left(\frac{-\hat s^2}{4\tau}\right)\Pi(0)}{M_{-1,0}^{\rm QCD}(\tau, s_0) + \Pi(0)} \tag{48}$$

$$N_{k}^{\rm QCD}(\hat s, \tau, s_0) \equiv \frac{G_{k}^{\rm QCD}(\hat s, \tau, s_0)}{M_{k,0}^{\rm QCD}(\tau, s_0)} \quad , \quad k \geq 0 \tag{49}$$

where the n-th moment of G_k is given by

$$M_{k,n}(\tau, s_0) = \int\limits_{-\infty}^{\infty} \hat s^n G_k(\hat s, \tau, s_0){\rm d}\hat s \quad , \quad n = 0, 1, 2, \ldots \quad . \tag{50}$$

---

[5] The role of higher-loop effects on the extraction of $\alpha\left(M_\tau\right)$ and the subsequent impact on $\Lambda_{\overline{MS}}$ has been investigated through Padé approximation techniques [18].

Note that, for the sake of notational convenience in subsequent sections, we have absorbed the low-energy theorem contribution into the definition of N_{-1}^{QCD} (see (48) above). This allows us to write our final version of the normalized Gaussian sum-rules of scalar gluonium as

$$N_k^{\text{QCD}}(\hat{s},\tau,s_0)=\frac{\frac{1}{\sqrt{4\pi\tau}}\int_{t_0}^{\infty}t^k\exp\left[\frac{-(\hat{s}-t)^2}{4\tau}\right]\frac{1}{\pi}\rho^{\text{had}}(t)\mathrm{d}t}{\int_{t_0}^{\infty}t^k\frac{1}{\pi}\rho^{\text{had}}(t)}\quad,\quad k\geq -1\quad. \tag{51}$$

Before describing analysis methods for the Gaussian sum-rules, we specify the numerical values for the QCD parameters appearing in (13) that will be employed in our analysis. For the dimension four gluon condensate, we make the assumption that $\langle J\rangle\approx\langle\alpha G^a_{\mu\nu}G^{a\mu\nu}\rangle$ and then employ the most recently updated value [21]

$$\langle\alpha G^a_{\mu\nu}G^{a\mu\nu}\rangle=(0.07\pm0.01)\ \text{GeV}^4\quad. \tag{52}$$

The dimension six gluon condensate can be related to $\langle\alpha G^a_{\mu\nu}G^{a\mu\nu}\rangle$ using instanton techniques (see [1, 22])

$$\langle\mathcal{O}_6\rangle=(0.27\ \text{GeV}^2)\langle\alpha G^a_{\mu\nu}G^{a\mu\nu}\rangle\quad. \tag{53}$$

Further, by invoking vacuum saturation in conjunction with the heavy quark expansion, the authors of [23] have related the dimension eight gluon condensate to $\langle\alpha G^a_{\mu\nu}G^{a\mu\nu}\rangle$ through

$$\langle\mathcal{O}_8\rangle=\frac{9}{16}\left(\langle\alpha G^a_{\mu\nu}G^{a\mu\nu}\rangle\right)^2\quad. \tag{54}$$

Regarding the instanton contributions, we shall employ Shuryak's dilute instanton liquid model [24] in which

$$n(\rho)=n_{\text{c}}\delta(\rho-\rho_{\text{c}}) \tag{55}$$

with

$$n_{\text{c}}=8.0\times10^{-4}\ \text{GeV}^4\ \text{and}\ \rho_{\text{c}}=\frac{1}{0.6}\ \text{GeV}^{-1}\quad. \tag{56}$$

3 Analysis of the Scalar Glueball Gaussian Sum-Rules

In most sum-rules analyses, it is necessary to make some assumptions concerning the hadronic content of the spectral function (34). A common choice in the literature is that of a single narrow resonance model. However, the wealth of scalar states with masses below 2 GeV [11], some of which are quite broad, certainly raises a question as to the validity of such an assumption, and suggest that a more general model allowing for a distribution of the resonance strength would be more suitable. In the following subsections, we show that this is indeed the case. Using appropriate generalizations of the analysis techniques developed in [9], we demonstrate that the single narrow resonance model provides an inadequate description of the hadronic content of the scalar glueball correlator, whereas certain distributed strength models lead to outstanding agreement between the theory and phenomenology parameterized by (51).

3.1 Single Narrow Resonance Model

In the single narrow resonance model, $\rho^{\text{had}}(t)$ takes the form

$$\rho^{\text{had}}(t)=\pi f^2\delta(t-m^2) \tag{57}$$

where m and f are respectively the resonance mass and coupling. With such an ansatz, the normalized Gaussian sum-rule (51) becomes

$$N_k^{\text{QCD}}(\hat{s},\tau,s_0)=\frac{1}{\sqrt{4\pi\tau}}\exp\left[-\frac{(\hat{s}-m^2)^2}{4\tau}\right]\quad. \tag{58}$$

The phenomenological side of (58) admits an absolute maximum (peak) located at $\hat{s} = m^2$, *independent* of τ; therefore, the theoretical side of (58) should mimic this behaviour provided that the single narrow resonance model (57) is actually an adequate description of hadronic physics below the continuum threshold (*i.e.* heavier states are weakly coupled enough to be absorbed into the continuum). Defining $\hat{s}_{\text{peak}}(\tau, s_0)$ by the condition

$$\frac{\partial}{\partial \hat{s}} N_k^{\text{QCD}}(\hat{s}_{\text{peak}}(\tau, s_0), \tau, s_0) = 0 \quad , \tag{59}$$

and denoting by $\{\tau_n\}_{n=0}^N$ an equally spaced partition of the τ interval of interest $[\tau_{\text{i}}, \tau_{\text{f}}]$ (we elaborate on this interval shortly), we define the following χ^2-function

$$\chi^2(s_0, m^2) = \sum_{n=0}^{N} \left[\hat{s}_{\text{peak}}(\tau_n, s_0) - m^2\right]^2 \tag{60}$$

as a measure of the difference between the theoretical peak position and the phenomenological peak position. Minimization of (60) with respect to s_0 and m^2 then provides us with values for these two parameters which correspond to the best possible fit between the theory and phenomenology as represented through (58). Lastly, the optimizing condition

$$\frac{\partial}{\partial m^2} \chi^2(s_0, m^2) = 0 \tag{61}$$

allows us to write m^2 as a function of s_0 whereby reducing (60) to a one-dimensional minimization problem:

$$\chi^2(s_0) = \sum_{n=0}^{N} \left[\hat{s}_{\text{peak}}(\tau_n, s_0) - m^2(s_0)\right]^2 \tag{62}$$

with

$$m^2(s_0) = \frac{1}{N+1} \sum_{n=0}^{N} \hat{s}_{\text{peak}}(\tau_n, s_0) \quad . \tag{63}$$

Thus, in a single narrow resonance analysis, we first minimize (62) with respect to s_0 to determine an optimum choice for the continuum threshold parameter and then substitute this value into (63) to obtain the best fit resonance mass.

Upon obtaining these optimized parameters, there exists criteria that can be used to assess the validity of this phenomenological model. For instance, if the single resonance analysis is a reasonable approach, plots of the theoretical Gaussian sum-rules (the left-hand side of (58)) and plots of the phenomenological Gaussian sum-rules (the right-hand side of (58)) should coincide (to a large degree). Significant deviation of one from the other may be indicative of an inadequate phenomenological model. On a more quantitative note, consider the following combination of moments (50) (where we suppress the explicit dependence on τ and s_0):

$$\sigma_k^2 \equiv \frac{M_{k,2}}{M_{k,0}} - \left(\frac{M_{k,1}}{M_{k,0}}\right)^2 \tag{64}$$

In the single narrow resonance model we should find

$$\sigma_k^2 - 2\tau = 0 \quad , \tag{65}$$

and hence a substantial deviation of $\sigma_k^2 - 2\tau$ from zero signals a failure of the single narrow resonance model.

To proceed with the analysis, however, we must first choose our region of interest $[\tau_{\text{i}}, \tau_{\text{f}}]$ needed in the definition of the χ^2 function (60). There are a number of factors to be considered in selecting this interval. The lower bound τ_{i} must be large enough such that the condensate contributions do not dominate perturbation theory and also such that the leading omitted perturbative term in the expansion for the running coupling (43) is small. Therefore, in accordance with these criteria, we choose a lower bound of $\tau_{\text{i}} \geq 2\ \text{GeV}^4$. To choose an appropriate upper bound on τ, we first note that the Gaussian kernel has a resolution of $\sqrt{2\tau}$. It is important to the analysis that the Gaussian sum-rules employed have a resolution less than the non-perturbative (hadronic physics) energy scale involved: roughly 2–3 GeV^2. This fact motivates an upper bound of $\tau_{\mathrm{f}} \leq 4\ \mathrm{GeV}^4$. Therefore, *in this and in all subsequent analyses*, we restrict our attention to the range $2\ \mathrm{GeV}^4 \leq \tau \leq\ 4\ \mathrm{GeV}^4$.

An analysis of the $k = -1$ normalized Gaussian sum-rule through (58) leads to predictions that are completely unstable under QCD uncertainties. Incorporating the error bounds of the dimension four gluonic condensate (52) and allowing for a 15% error in each of n_{c} and ρ_{c} leads to a huge degree of variation in the resulting hadronic parameter estimates, and it is not even possible to ascertain whether or not an extension of the single resonance analysis is warranted. Mass predictions range anywhere from 1.0 GeV to 1.8 GeV, an interval far too broad to be of much use. The only inference we can draw from $k = -1$ analysis is that the mass scale obtained is in rough agreement with that which results from an analysis of the next-to-leading order ($k = 0$) Gaussian sum-rule (see below). We note further that this consistency in mass scales between the $k = -1$ and higher order sum-rules is also observed in [5, 6] and occurs only when instanton effects are included. Due to its extreme sensitivity to small variations in various QCD parameters, we are forced to conclude that the $k = -1$ Gaussian sum-rule is an unreliable probe of the scalar glueball sector, and so, move on to a $k = 0$ analysis.

A single narrow resonance analysis of the $k = 0$ Gaussian sum-rule, however, leads to rather poor agreement between theory and phenomenology. Minimization of (62) leads to an optimum threshold at $s_0 = 2.3\ \mathrm{GeV}^2$ which, when substituted into (63), yields a resonance mass of $m = 1.30$ GeV. In Figure 3, we plot both $\sigma_0^2(\tau, s_0)$ and 2τ versus τ for $s_0 = 2.3\ \mathrm{GeV}^2$. The graph of $\sigma_0^2(\tau, s_0)$ appears to have a slope of two, but, if extended to $\tau = 0$, would not pass through the origin—a situation which contradicts the single resonance result (65). Further, in Figure 4, we plot the left- (theoretical) and right- (phenomenological) hand sides of (58) versus $\hat{s}$ for $\tau \in \{2, 3, 4\}\ \mathrm{GeV}^4$ using the optimized values $m = 1.30$ GeV and $s_0 = 2.3\ \mathrm{GeV}^2$. The discrepancy between theory and phenomenology is apparent: the theoretical curves consistently underestimate phenomenology near the peak and overestimate phenomenology in the tails. These observations indicate that a single narrow resonance ansatz is an inadequate description of the scalar gluonium spectral function, hence motivating our subsequent analyses of more general models.

3.2 Distributed Resonance Strength Models

The moment combination σ_k^2 measures the width of the QCD distribution, and since $\sigma_0^2 - 2\tau > 0$, we conclude that the resonance strength is distributed over an energy region broad enough to be sampled by the resolution $\sqrt{2\tau}$ of the Gaussian kernel. In accordance, we should therefore consider phenomenological models which allow for such a spreading. We focus on three distinct classes of distributed strength models:

1. single non-zero width models,
2. a double narrow resonance model, and
3. single narrow resonance + single non-zero width resonance models,

ordered according to increasing complexity, *i.e.* the (normalized) single non-zero width models each contain two free parameters whereas the single narrow resonance + single non-zero width models requires four. In the subsections to follow, we outline the analysis procedure and the resulting hadronic parameter predications corresponding to each of the models under consideration.

3.2.1 Single Non-Zero Width Models

The first non-zero width model we consider is a unit-area square pulse representing a broad, structureless background which has previously been used for the study of the σ resonance [25]. To describe such a square pulse centred at m^2 and having width $2m\Gamma$, we define

$$\frac{1}{\pi}\rho^{\mathrm{had}}(t) = \frac{1}{\pi}\rho^{sp}(t) \equiv \frac{1}{2m\Gamma}\left[\theta\left(t - m^2 + m\Gamma\right) - \theta\left(t - m^2 - m\Gamma\right)\right] \quad , \tag{66}$$

which leads to the following normalized Gaussian sum-rule (51) for $k=0$:

$$N_0^{\rm QCD}(\hat{s},\tau,s_0)=\frac{1}{4m\Gamma}\left[\operatorname{erf}\left(\frac{\hat{s}-m^2+m\Gamma}{2\sqrt{\tau}}\right)-\operatorname{erf}\left(\frac{\hat{s}-m^2-m\Gamma}{2\sqrt{\tau}}\right)\right]\quad . \tag{67}$$

As in the single narrow resonance analysis, the phenomenological side of (67) admits a single τ-independent peak, and so we can determine an optimum threshold parameter s_0 by following the steps outlined through (60)–(63) *i.e.* $s_0=2.3\ {\rm GeV}^2$. We wish to use this optimized value of s_0 to generate predictions for the hadronic parameters $\{m,\,\Gamma\}$. The following combinations of the moments (50) (where we suppress the explicit dependence on τ and s_0) are useful in this regard:

$$\begin{gathered}\frac{M_{k,1}}{M_{k,0}}\quad,\quad \sigma_k^2\equiv\frac{M_{k,2}}{M_{k,0}}-\left(\frac{M_{k,1}}{M_{k,0}}\right)^2\\ A_k^{(3)}\equiv\frac{M_{k,3}}{M_{k,0}}-3\left(\frac{M_{k,2}}{M_{k,0}}\right)\left(\frac{M_{k,1}}{M_{k,0}}\right)+2\left(\frac{M_{k,1}}{M_{k,0}}\right)^3\quad .\end{gathered} \tag{68}$$

In the spirit of the sum-rules approach, we equate each of these theoretical quantities to its corresponding phenomenological counterpart resulting in the following system of equations:

$$\frac{M_{0,1}}{M_{0,0}}=m^2 \tag{69}$$

$$\sigma_0^2-2\tau=\frac{1}{3}m^2\Gamma^2 \tag{70}$$

$$A_0^{(3)}=0\quad . \tag{71}$$

Considering that the right-hand (phenomenological) sides of (69)–(71) are all τ-independent, it is an important feature of the analysis that, at the optimized continuum threshold s_0, the left-hand (theoretical) sides exhibit negligible dependence on τ and so are well approximated throughout the interval $[\tau_{\rm i},\tau_{\rm f}]$ by averaged values. Such τ-independence of appropriate residual moment combinations also occurs in the more complicated models considered below.

Then, we can use (69)–(70) to obtain predictions for the two free parameters $\{m,\,\Gamma\}$ of the square pulse model (66). Equation (71) is independent of our parameter estimates and therefore serves as an *a posteriori* consistency test.[6]

Inverting (69)–(70), we obtain $m=(1.30\pm0.17)$ GeV and $\Gamma=(0.59\pm0.07)$ GeV, where, in this and in all subsequent analyses, the uncertainties quoted stem from the error bounds on the dimension-four gluonic condensate (52) and an estimated 15% uncertainty in each of $n_{\rm c}$ and $\rho_{\rm c}$ (see (56)). In Figure 5, we use $s_0=2.3\ {\rm GeV}^2$ and central values of m and Γ to plot the theoretical and phenomenological sides of (67) versus $\hat{s}$ for $\tau\in\{2,3,4\}\ {\rm GeV}^4$. The excellent agreement between theory and phenomenology demonstrated by these plots is a vast improvement over the results of the $k=0$ single narrow resonance analysis (see Figure 4).

However, closer quantitative scrutiny reveals that the fits depicted in Figure 5 are not quite as accurate as one might think. The quantity $A_0^{(3)}$ involves higher order moments of the $k=0$ Gaussian sum-rule and so is sensitive to an even finer level of detail than are $M_{0,1}/M_{0,0}$ and σ_0^2. A QCD calculation of this quantity yields $A_0^{(3)}=-0.0825\,{\rm GeV}^6$ in significant violation of our consistency check (71).

For our second example of a single non-zero width model, we would ideally like to consider a Breit-Wigner resonance. However, closed-form expressions do not exist for the Gaussian image of a Breit-Wigner shape, and so we instead employ a Gaussian model to describe a well-defined resonance peak with a non-zero width

$$\rho^{\rm had}(t)=\rho^{\rm g}(t)\equiv f_g^2\exp\left[-\frac{\left(t-m^2\right)^2}{2\Gamma^2}\right]\quad . \tag{72}$$

---

[6] For the square pulse model, it seems we could use either (69) or (63) to compute the mass m; however, as we shall see, both yield the same result. We concentrate on (69) simply because the analysis techniques outlined here are easily generalized to the more complicated resonance models to follow.

The quantity f_g^2 is a normalization constant related to the total resonance strength, and the Gaussian width Γ is related to an equivalent Breit-Wigner width Γ_{BW} through

$$\Gamma_{BW} = \sqrt{2\log 2}\frac{\Gamma}{m} \quad . \tag{73}$$

In this model, the $k = 0$ normalized Gaussian sum-rule (51) becomes

$$N_0^{\rm QCD}(\hat{s},\tau,s_0) = \frac{1+{\rm erf}\left(\frac{\hat{s}\Gamma^2+2m^2\tau}{2\Gamma\sqrt{\tau}\sqrt{\Gamma^2+2\tau}}\right)}{\sqrt{2\pi}\sqrt{\Gamma^2+2\tau}\left[1+{\rm erf}\left(\frac{m^2}{\sqrt{2}\Gamma}\right)\right]}\exp\left[-\frac{\left(\hat{s}-m^2\right)^2}{2\left(\Gamma^2+2\tau\right)}\right] \quad , \tag{74}$$

where

$${\rm erf}(x) = \frac{2}{\sqrt{\pi}}\int\limits_0^x e^{-y^2}\,dy \quad . \tag{75}$$

As in prior analyses, we begin with an extraction of the optimized continuum threshold parameter s_0, and again, we accomplish this by examining the behaviour or the peak position. The phenomenological side of (74) admits a single peak; however, in contrast to our previous two analyses, *the position of this peak is dependent on* τ. Differentiating the right-hand side of (74) and setting the result to zero gives

$$\hat{s}-m^2 = \frac{\Gamma}{\sqrt{\pi\tau}}\left[\frac{\exp\left(-\frac{\left(\hat{s}\Gamma^2+2m^2\tau\right)^2}{4\Gamma^2\tau(\Gamma^2+2\tau)}\right)}{1+{\rm erf}\left(\frac{\hat{s}\Gamma^2+2m^2\tau}{2\Gamma\sqrt{\tau}\sqrt{\Gamma^2+2\tau}}\right)}\right] \tag{76}$$

which, unfortunately cannot be explicitly solved for $\hat{s}$. Consequently, in the absence of an exact solution, we approximate the phenomenological peak position by the expression

$$A+\frac{B}{\tau}+\frac{C}{\tau^2} \tag{77}$$

where $\{A,B,C\}$ are to be considered unknown parameters. Explicit numerical experiments in (realistic) worst-case scenarios show that, provided $\tau \geq 2$ GeV^4, the next term in the expansion (77) [*i.e.* D/τ^3] is negligible and can safely be ignored. Therefore, we are led to define the following χ^2-function as a measure of the deviation of the theoretical peak position (59) from the phenomenological peak position characterized by the expansion (77):

$$\chi^2(s_0,A,B,C) = \sum_{n=0}^{N}\left[\hat{s}_{\rm peak}(\tau_n,s_0)-A-\frac{B}{\tau_n}-\frac{C}{\tau_n^2}\right]^2 \quad . \tag{78}$$

The χ^2 minimizing conditions

$$\frac{\partial\chi^2}{\partial A} = \frac{\partial\chi^2}{\partial B} = \frac{\partial\chi^2}{\partial C} = 0 \tag{79}$$

can then be used to write $\{A,B,C\}$ as functions[7] of s_0 leaving us with a one-dimensional minimization problem in s_0:

$$\chi^2(s_0) = \sum_{n=0}^{N}\left[\hat{s}_{\rm peak}(\tau_n,s_0)-A(s_0)-\frac{B(s_0)}{\tau_n}-\frac{C(s_0)}{\tau_n^2}\right]^2 \quad . \tag{80}$$

---

[7] The set of equations defined by condition (79) is linear and inhomogeneous. While trivial to obtain, the solution is rather a mess and so is omitted for brevity.

Minimizing (80) with respect to s_0 furnishes us with an optimized choice for the continuum threshold parameter.

Once the optimized s_0 has been determined, the subsequent analysis of the Gaussian resonance model proceeds in a fashion completely analogous to the analysis of the square pulse model. For instance, the appropriate Gaussian model equations corresponding to (69)–(71) are

$$\frac{M_{0,1}}{M_{0,0}} = m^2 + \Gamma\Delta \tag{81}$$

$$\sigma_0^2 - 2\tau = \Gamma^2 - m^2\Gamma\Delta - \Gamma^2\Delta^2 \tag{82}$$

$$A_0^{(3)} = \left(m^4\Gamma - \Gamma^3\right)\Delta + 3m^2\Gamma^2\Delta^2 + 2\Gamma^3\Delta^3 \tag{83}$$

where

$$\Delta = \sqrt{\frac{2}{\pi}}\left[\frac{\exp\left(-\frac{m^4}{2\Gamma^2}\right)}{1+\mathrm{erf}\left(\frac{m^2}{\sqrt{2}\Gamma}\right)}\right] \quad . \tag{84}$$

Again, the first two equations may be (numerically) inverted to yield predictions for the model's two free parameters $\{m, \Gamma\}$ while the third serves as an independent consistency check. The quantity Δ is small, and hence the terms in (81–83) proportional to Δ have a negligible effect on the extracted resonance parameters, a property which also simplifies our subsequent analysis. Note that since $A_0^{(3)} \sim \Delta$ in (83), we anticipate that this model will still underestimate the QCD value of this moment combination, a result which is confirmed in our detailed analysis.

Carrying out the appropriate sequence of calculations first gives an optimized continuum threshold parameter[8] $s_0 = 2.3\ \mathrm{GeV}^2$ which, in turn, yields a mass of $m = (1.30 \pm 0.17)$ GeV and an equivalent Breit-Wigner width (see (73)) of $\Gamma_{\mathrm{BW}} = (0.40 \pm 0.05)$ GeV. Again, we test the validity of these values by plotting both the theoretical and phenomenological sides of (74) versus $\hat{s}$ for $\tau \in \{2, 3, 4\}\ \mathrm{GeV}^4$, setting $s_0 = 2.3\ \mathrm{GeV}^2$ and employing the central values of the resonance parameters. The resulting graphs are, to the naked eye, indistinguishable from those corresponding to the square pulse model analysis[9] (Figure 5) and so are omitted.

Substitution of the central values of m and Γ into (83) yields $A_0^{(3)} = 0.000342\,\mathrm{GeV}^6$ which must again be compared with the QCD value of $A_0^{(3)} = -0.0825\,\mathrm{GeV}^6$. Clearly, there exists a significant discrepancy between the two as the Gaussian model cannot even correctly predict the sign of this moment combination.

The quantity $A_0^{(3)}$, however, is a measure of the asymmetry of $N_0^{\mathrm{QCD}}(\hat{s}, \tau, s_0)$ with respect to $\hat{s}$ about its average value defined by $M_{0,1}/M_{0,0}$. Therefore, considering that both the Gaussian and square pulse models represent resonance strength distributions that are symmetric (about m^2), it is perhaps not surprising that they fail to accurately predict $A_0^{(3)}$. Hence, we are prompted to consider a skewed generalization of the Gaussian resonance model:

$$\rho^{\mathrm{had}}(t) = \rho^{\mathrm{sg}}(t) \equiv t^2 f^2 \exp\left[-\frac{(t-m^2)^2}{2\Gamma^2}\right] \tag{85}$$

where the factor t^2 introduces a degree of asymmetry and has been chosen to achieve consistency with known low-energy two pion decay rates [10, 26]. Substituting (85) into (51) gives

$$\begin{aligned} E\, N_0^{\mathrm{QCD}}(\hat{s}, \tau, s_0) = {} & 2\sqrt{\pi}\exp\left[-\frac{(\hat{s}-m^2)^2}{2(\Gamma^2+2\tau)}\right]\left(\hat{s}^2\Gamma^4 + 4\hat{s}\Gamma^2 m^2\tau + 4m^4\tau^2 + 2\tau\Gamma^4 + 4\tau^2\Gamma^2\right)\left[1+\mathrm{erf}\left(\frac{\hat{s}\Gamma^2 + 2\tau m^2}{2\Gamma\sqrt{\tau}\sqrt{\Gamma^2+2\tau}}\right)\right] \\ & + 4\exp\left[-\frac{\hat{s}^2\Gamma^2 + 2\tau m^4}{4\tau\Gamma^2}\right]\Gamma\sqrt{\tau}\sqrt{\Gamma^2+2\tau}\left(\hat{s}\Gamma^2 + 2\tau m^2\right) \end{aligned} \tag{86}$$

where

$$E = \sqrt{2\pi}(m^4+\Gamma^2)\left[1+\mathrm{erf}\left(\frac{m^2}{\sqrt{2}\Gamma}\right)\right] + 2m^2\Gamma\exp\left(-\frac{m^4}{2\Gamma^2}\right)\sqrt{\pi}(\Gamma^2+2\tau)^{5/2} \quad . \tag{87}$$

---

[8] Surprisingly, this is the same optimized threshold parameter value that we found in the single narrow resonance model analysis. This need not always be the case as depicted explicitly in [9].

[9] We quantitatively address this situation in Section 4.

The sum-rules analysis proceeds along the same lines as for the unskewed Gaussian resonance model. The appropriate generalizations of (81)–(83) are

$$\frac{M_{0,1}}{M_{0,0}} = \frac{m^2(m^4+3\Gamma^2)}{m^4+\Gamma^2} + \mathcal{O}(\Delta) \tag{88}$$

$$\sigma_0^2 - 2\tau = \frac{\Gamma^2(m^8+3\Gamma^4)}{(m^4+\Gamma^2)^2} + \mathcal{O}(\Delta) \tag{89}$$

$$A_0^{(3)} = \frac{4m^2\Gamma^6(m^4-3\Gamma^2)}{(m^4+\Gamma^2)^3} + \mathcal{O}(\Delta) \tag{90}$$

Numerically inverting[10] (88)–(89), we find a mass $m = (1.17 \pm 0.15)\,\mathrm{GeV}$ and an equivalent Breit-Wigner width of $\Gamma_{\mathrm{BW}} = (0.49 \pm 0.06)\,\mathrm{GeV}$. A subsequent phenomenological prediction yields $A_0^{(3)} = 0.00943\,\mathrm{GeV}^6$—again, completely inaccurate compared with the QCD value. These results, as well as the results of the unskewed non-zero resonance width model analyses are summarized for convenience in Table 1.

resonance model	mass (GeV)	width (GeV)	$A_0^{(3)}$ (GeV^6)
unskewed Gaussian	1.30	0.38	0.000342
unskewed square pulse	1.30	0.59	0
skewed Gaussian	1.18	0.49	0.00943

Table 1: The results of a $k = 0$ Gaussian sum-rules analysis of a variety of non-zero resonance width models using central values of the QCD parameters. For the Gaussian resonance models, the given width is actually the equivalent Breit-Wigner width (see (73)). The $A_0^{(3)}$ values should be compared with the QCD prediction $A_0^{(3)} = -0.0825\,\mathrm{GeV}^6$.

3.2.2 Double Narrow Resonance Model

The double narrow resonance model is defined by

$$\rho^{\mathrm{had}}(t) = \rho^{2\mathrm{r}}(t) \equiv \pi\left[f_1^2\delta(t-m_1^2) + f_2^2\delta(t-m_2^2)\right] \tag{91}$$

where $m_1 \leq m_2$ are the two resonance masses and f_1, f_2 are their respective couplings. Correspondingly, the normalized Gaussian sum-rule (51) reduces to

$$N_k^{\mathrm{QCD}}(\hat{s},\tau,s_0) = \frac{1}{\sqrt{4\pi\tau}}\left\{\frac{f_1^2m_1^{2k}}{f_1^2m_1^{2k}+f_2^2m_2^{2k}}\exp\left[-\frac{(\hat{s}-m_1^2)^2}{4\tau}\right] + \frac{f_2^2m_2^{2k}}{f_1^2m_1^{2k}+f_2^2m_2^{2k}}\exp\left[-\frac{(\hat{s}-m_2^2)^2}{4\tau}\right]\right\} \quad . \tag{92}$$

In the analysis of this model, it becomes inconvenient to use the parameters $\{m_1, f_1, m_2, f_2\}$ and so we instead focus on the set $\{z, y, r\}$ defined by

$$z = m_1^2 + m_2^2 \quad , \quad y = m_1^2 - m_2^2 \quad , \quad r = r_1 - r_2 \tag{93}$$

with

$$r_1 = \frac{f_1^2m_1^{2k}}{f_1^2m_1^{2k}+f_2^2m_2^{2k}} \quad , \quad r_2 = \frac{f_2^2m_2^{2k}}{f_1^2m_1^{2k}+f_2^2m_2^{2k}} \quad \text{with} \quad r_1 + r_2 = 1 \quad . \tag{94}$$

As in the Gaussian resonance model analysis, the phenomenological side of (92) admits a single peak whose position is τ-dependent. In terms of the double resonance model parameters (93), differentiating the right-hand side of (92) with respect to $\hat{s}$ and setting the result to zero yields

$$\frac{(r+1)\left(\hat{s}-\frac{1}{2}z-\frac{1}{2}y\right)}{(r-1)\left(\hat{s}-\frac{1}{2}z+\frac{1}{2}y\right)} - \exp\left[\frac{y\,(z-2\hat{s})}{4\tau}\right] = 0 \tag{95}$$

---

[10] The terms in (88)–(89) proportional to Δ are found to have a negligible impact on the solutions.

which, again, cannot be explicitly solved for $\hat{s}$. Thus, we approximate the phenomenological peak position by the expression (77) and correspondingly, extract an optimized continuum threshold parameter $s_0 = 2.3\ \mathrm{GeV}^2$.

To compute predictions for the hadronic parameters of the double narrow resonances model, we again look to moment combinations such as (68). However, since this model contains three free parameters (93), we require three equations. In other words, if we wish to have an independent consistency check of our results, we must introduce a fourth moment combination in addition to those of (68). Defining

$$S_k \equiv \frac{M_{k,4}}{M_{k,0}} - 4\frac{M_{k,3}}{M_{k,0}}\frac{M_{k,1}}{M_{k,0}} + 6\frac{M_{k,2}}{M_{k,0}}\left(\frac{M_{k,1}}{M_{k,0}}\right)^2 - 3\left(\frac{M_{k,1}}{M_{k,0}}\right)^4 \tag{96}$$

leads to the following equations

$$\frac{M_{k,1}}{M_{k,0}} = \frac{1}{2}(z + ry) \tag{97}$$

$$\sigma_k^2 - 2\tau = \frac{1}{4}y^2(1 - r^2) \tag{98}$$

$$A_k^{(3)} = -\frac{1}{4}ry^3(1 - r^2) \tag{99}$$

$$S_k - 12\tau^2 - 12\tau\left(\sigma_k^2 - 2\tau\right) = \frac{1}{16}y^4\left(1 - r^2\right)\left(1 + 3r^2\right) \quad . \tag{100}$$

which are analogous to (69)–(71) and (81)–(83).

For the $k = 0$ case of interest, upon inverting (97)–(99) we find the heavier of the two states is also the more strongly coupled with $m_2 = (1.4 \pm 0.2)$ GeV and $r_2 = 0.72 \pm 0.06$. The lighter resonance with a mass $m_1 = (0.98 \pm 0.2)$ GeV is the more weakly coupled state with $r_1 = 0.28 \mp 0.06$. The QCD uncertainties given for the resonance masses obscure the very stable mass splitting between the two states: $m_2 - m_1 = (0.42 \pm 0.03)$ GeV. Again, plots of the theoretical and phenomenological Gaussian sum-rules exhibit the excellent agreement shown in Figure 5.

Using central values of the hadronic parameters obtained, we can calculate a phenomenological prediction associated with the first independent moment combination (96). The result is $S_0 - 12\tau^2 - 12\tau\left(\sigma_0^2 - 2\tau\right) = 0.073733\,\mathrm{GeV}^8$ which must compared with a QCD calculation of $S_0 - 12\tau^2 - 12\tau\left(\sigma_0^2 - 2\tau\right) = 0.169769\,\mathrm{GeV}^8$. The roughly 50% deviation between these values is a large improvement over similar comparisons in the single non-zero width resonance models.

3.2.3 Two Resonance Model of a Narrow Resonance Combined with a Wide Resonance

A natural extension of the double narrow resonance model is to introduce an additional parameter into the hadronic model which describes the width for one of the resonances.

We begin with a model consisting of a narrow resonance of mass m and a Gaussian resonance of mass M and width Γ. The resulting $k = 0$ normalized Gaussian sum-rule (51) is:

$$N_0^{\mathrm{QCD}}\left(\hat{s}, \tau, s_0\right) = r_m \frac{1}{\sqrt{4\pi\tau}} \exp\left[-\frac{(\hat{s} - m^2)^2}{4\tau}\right] + r_M \exp\left(-\frac{\left(\hat{s} - M^2\right)^2}{2\left(\Gamma^2 + 2\tau\right)}\right)\left[\frac{1 + \mathrm{erf}\left(\frac{\hat{s}\Gamma^2 + 2M^2\tau}{2\Gamma\sqrt{\tau}\sqrt{\Gamma^2 + 2\tau}}\right)}{\sqrt{2\pi}\sqrt{\Gamma^2 + 2\tau}\left[1 + \mathrm{erf}\left(\frac{M^2}{\sqrt{2}\Gamma}\right)\right]}\right] \quad , \tag{101}$$

where r_m and r_M denote the relative strengths of the resonances and are constrained by $r_m + r_M = 1$. As in the other models, the phenomenological side of (101) has a single τ-dependent peak position. The peak-drift χ^2 in (78) is again minimized to find the optimum value of the continuum, and then the theoretical (QCD) values for the moments are used to determine the resonance parameters. Since this model contains four independent parameters, the lowest four moment combinations (68,96) are used to determine the parameters and the following fifth order moment combination will be used as a consistency check.

$$A_k^{(5)} = \frac{M_{k,5}}{M_{k,0}} - 5\frac{M_{k,4}}{M_{k,0}}\frac{M_{k,1}}{M_{k,0}} + 10\frac{M_{k,3}}{M_{k,0}}\left(\frac{M_{k,1}}{M_{k,0}}\right)^2 - 10\frac{M_{k,2}}{M_{k,0}}\left(\frac{M_{k,1}}{M_{k,0}}\right)^3 + 4\left(\frac{M_{k,1}}{M_{k,0}}\right)^5 \tag{102}$$

Defining

$$z = M^2 + m^2 \quad , \quad y = m^2 - M^2 \quad , \quad r = r_m - r_M \tag{103}$$

we find the following expressions for the moment combinations in terms of the resonance parameters

$$\frac{M_{0,1}}{M_{0,0}} = \frac{1}{2}\left(z + ry\right) + \mathcal{O}\left(\Delta\right) \tag{104}$$

$$\sigma_0^2 - 2\tau = \frac{1}{4}y^2\left(1 - r^2\right) + \frac{1}{2}\Gamma^2\left(1 - r\right) + \mathcal{O}\left(\Delta\right) \tag{105}$$

$$A_0^{(3)} = -\frac{1}{4}y^3 r\left(1 - r^2\right) - \frac{3}{4}\Gamma^2 y\left(1 - r^2\right) + \mathcal{O}\left(\Delta\right) \tag{106}$$

$$S_0 - 12\tau^2 - 12\tau\left(\sigma_0^2 - 2\tau\right) = \frac{1}{16}y^4\left(1 - r^2\right)\left(1 + 3r^2\right) + \frac{3}{4}\Gamma^2 y^2\left(1 + r\right)\left(1 - r^2\right) + \frac{3}{2}\Gamma^4\left(1 - r\right) + \mathcal{O}\left(\Delta\right) \tag{107}$$

$$A_0^{(5)} - 20\tau A_0^{(3)} = -\frac{1}{8}y^5 r\left(1 - r^2\right)\left(1 + r^2\right) - \frac{5}{8}\Gamma^2 y^3\left(1 - r\right)\left(1 + r\right)^3 - \frac{15}{4}\Gamma^4 y\left(1 - r^2\right) + \mathcal{O}\left(\Delta\right) \tag{108}$$

The terms proportional to Δ (see equation (84)) in the above expressions are found to be numerically insignificant.

The QCD values of the moments are used to solve (104–107) for the resonance parameters.[11] The non-linear nature of (104–107) might suggest a large number of solutions, but it is found that only one physical solution persists across the range of QCD parameters considered: $m = (1.41 \pm 0.19)\,\mathrm{GeV}$, $M = (1.23 \pm 0.15)\,\mathrm{GeV}$, $\Gamma_{BW} = (0.52 \pm 0.06)\,\mathrm{GeV}$, $r_m = 0.49 \pm 0.13$, $r_M = 1 - r_m$. Plots of the theoretical and phenomenological sides of the normalized Gaussian sum-rules are again represented in Figure 5, illustrating excellent agreement between the QCD prediction and phenomenological model.

The fifth-order moment (108) can now be used as a consistency check. The resonance parameters for the central QCD parameters yields $A_0^{(5)} - 20\tau A_0^{(3)} = -0.130\,\mathrm{GeV}^{10}$ which should be compared with the QCD value of $A_0^{(5)} - 20\tau A_0^{(3)} = -0.243\mathrm{GeV}^{10}$.

To assess whether other non-zero width models lead to better agreement with the QCD value of $A_0^{(5)} - 20\tau A_0^{(3)} = -0.243\,\mathrm{GeV}^{10}$ we consider using the square pulse model instead of the Gaussian resonance, which results in a normalized Gaussian sum-rule similar to (101)

$$N_0^{\mathrm{QCD}}(\hat{s}, \tau, s_0) = r_m \frac{1}{\sqrt{4\pi\tau}} \exp\left[-\frac{(\hat{s} - m^2)^2}{4\tau}\right] + r_M \frac{1}{4M\Gamma}\left[\mathrm{erf}\left(\frac{\hat{s} - M^2 + M\Gamma}{2\sqrt{\tau}}\right) - \mathrm{erf}\left(\frac{\hat{s} - M^2 - M\Gamma}{2\sqrt{\tau}}\right)\right] \quad , \tag{109}$$

where $r_m + r_M = 1$. Using the definitions (103) results in the following expressions for the moment combinations in terms of the resonance parameters.

$$\frac{M_{0,1}}{M_{0,0}} = \frac{1}{2}\left(z + ry\right) + \mathcal{O}\left(\Delta\right) \tag{110}$$

$$\sigma_0^2 - 2\tau = \frac{1}{4}y^2\left(1 - r^2\right) + \frac{1}{12}\Gamma^2\left(z - y\right)\left(1 - r\right) + \mathcal{O}\left(\Delta\right) \tag{111}$$

$$A_0^{(3)} = -\frac{1}{4}y^3 r\left(1 - r^2\right) - \frac{1}{8}\Gamma^2 y\left(1 - r^2\right)\left(z - y\right) + \mathcal{O}\left(\Delta\right) \tag{112}$$

$$\begin{aligned} S_0 - 12\tau^2 - 12\tau\left(\sigma_0^2 - 2\tau\right) =& \frac{1}{16}y^4\left(1 - r^2\right)\left(1 + 3r^2\right) + \frac{1}{8}\Gamma^2 y^2\left(1 + r\right)\left(1 - r^2\right)\left(z - y\right) \\ &+ \frac{1}{40}\Gamma^4\left(1 - r\right)\left(z - y\right)^2 + \mathcal{O}\left(\Delta\right) \end{aligned} \tag{113}$$

$$\begin{aligned} A_0^{(5)} - 20\tau A_0^{(3)} =& -\frac{1}{8}y^5 r\left(1 - r^2\right)\left(1 + r^2\right) - \frac{5}{48}\Gamma^2 y^3\left(1 - r^2\right)\left(1 + r\right)^2\left(z - y\right) \\ &- \frac{1}{16}\Gamma^4 y\left(1 - r^2\right)\left(z - y\right)^2 + \mathcal{O}\left(\Delta\right) \end{aligned} \tag{114}$$

---

[11] As mentioned earlier, the QCD value of the residual moment combinations are found to be virtually τ independent consistent with the resonance model expressions (104–108).

Using the QCD values of the moments to solve (110–113) for the resonance parameters again yields a single physical solution over the QCD parameter space: $m = (1.33 \pm 0.18)\,\mathrm{GeV}$, $M = (1.23 \pm 0.18)\,\mathrm{GeV}$, $\Gamma_{BW} = (0.95 \pm 0.12)\,\mathrm{GeV}$, $r_m = 0.60 \pm 0.13$, $r_M = 1 - r_m$. Agreement between the theoretical and phenomenological sides of the normalized Gaussian sum-rules is again excellent, as exhibited by the plots shown in Figure 5.

The value of the fifth-order moment combination (114) for the resonance parameters corresponding to the central QCD parameters is $A_0^{(5)} - 20\tau A_0^{(3)} = -0.114\,\mathrm{GeV}^{10}$. The square pulse model is thus not an improvement upon the Gaussian resonance model's agreement with the QCD value of this residual moment combination.

As a final scenario, we modify the normalized Gaussian sum-rule of (101) for a skewed Gaussian resonance

$$\begin{aligned} N_0^{\mathrm{QCD}}(\hat{s},\tau,s_0) =& r_m \frac{1}{\sqrt{4\pi\tau}} \exp\left[-\frac{(\hat{s}-m^2)^2}{4\tau}\right] \\ &+ \frac{r_M}{E} 2\sqrt{\pi} \exp\left[-\frac{(\hat{s}-M^2)^2}{2(\Gamma^2+2\tau)}\right] \left(\hat{s}^2\Gamma^4 + 4\hat{s}\Gamma^2 M^2\tau + 4M^4\tau^2 + 2\tau\Gamma^4 + 4\tau^2\Gamma^2\right) \left[1 + \mathrm{erf}\left(\frac{\hat{s}\Gamma^2 + 2\tau M^2}{2\Gamma\sqrt{\tau}\sqrt{\Gamma^2+2\tau}}\right)\right] \\ &+ \frac{r_M}{E} 4 \exp\left[-\frac{\hat{s}^2\Gamma^2 + 2\tau M^4}{4\tau\Gamma^2}\right] \Gamma\sqrt{\tau}\sqrt{\Gamma^2+2\tau}(\hat{s}\Gamma^2 + 2\tau M^2) \end{aligned} \tag{115}$$

where E (with appropriate substitution of the mass M) is defined in (87). Using the same conventions, we obtain lengthy expressions for the moment combinations in terms of the resonance parameters.

$$D\frac{M_{0,1}}{M_{0,0}} = \frac{1}{2}(z+ry)(z-y)^2 + \Gamma^2(-2y+4z+4ry-2rz) + \mathcal{O}(\Delta) \tag{116}$$

$$D = (z-y)^2 + 4\Gamma^2 \tag{117}$$

$$\begin{aligned} D^2\left(\sigma_0^2 - 2\tau\right) =& \frac{1}{4}y^2\left(1-r^2\right)(z-y)^4 + \frac{1}{2}\Gamma^2(1-r)(z-y)^2\left(z^2 - 4ryz - 6yz + 9y^2 + 8ry^2\right) \\ &+ 4\Gamma^4\left(1-r^2\right)(z-2y)^2 + 24\Gamma^6(1-r) + \mathcal{O}(\Delta) \end{aligned} \tag{118}$$

$$\begin{aligned} D^3A_0^{(3)} =& -\frac{1}{4}y^3r\left(1-r^2\right)(z-y)^6 - \frac{3}{4}\Gamma^2y\left(1-r^2\right)(z-y)^4\left(z^2 - 4zry - 2yz + 8ry^2 + y^2\right) \\ &+ 3\Gamma^4\left(1-r^2\right)(z-y)^2(z-2y)\left(z^2 - 4zry - 2yz + 8ry^2 + y^2\right) \\ &+ 4\Gamma^6(1-r)\left[y^3\left(-32r^2 - 41r - 13\right) + z^3 4\left(r^2 + r + 1\right) + y^2 z 6\left(8r^2 + 11r + 5\right) + z^2 y\left(-24r^2 - 33r - 21\right)\right] \\ &+ 48\Gamma^8(1-r)(-6ry + 3rz - 2y - z) + \mathcal{O}(\Delta) \end{aligned} \tag{119}$$

$$
\begin{aligned}
D^4\left[S_0-12\tau^2-12\tau\left(\sigma_0^2-2\tau\right)\right] &= \frac{1}{16}y^4\left(1-r^2\right)\left(1+3r^2\right)(z-y)^8\\
&+\frac{1}{4}\Gamma^2y^2\left(1-r^2\right)(z-y)^8\left(3rz^2+3z^2-6zry-12zr^2y-10yz+24r^2y^2+11y^2+3ry^2\right)\\
&+\frac{3}{2}\Gamma^4(1-r)(z-y)^4\left[z^4+y^4\left(48r^3+56r^2+32r+25\right)+yz^3\left(-4r^2-8r-8\right)+y^3z\left(-48r^3-68r^2-56r-40\right)\right.\\
&\qquad\left.+y^2z^2\left(12r^3+28r^2+36r+26\right)\right]\\
&+4\Gamma^6\left(1-r^2\right)(z-y)^2\left[z^43(1+r)+y^4\left(96r^2+21r+61\right)+yz^3\left(-12r^2-18r-30\right)+y^3z\left(-144r^2-54r-126\right)\right.\\
&\qquad\left.+y^2z^2\left(72r^2+48r+96\right)\right]\\
&+16\Gamma^8(1-r)\left[z^4\left(3r^3+3r^2+9r+12\right)+y^4\left(48r^3+84r^2+80r+47\right)+y^3z\left(-96r^3-186r^2-196r-118\right)\right.\\
&\qquad\left.+z^3y\left(-24r^3-42r^2-60r-54\right)+y^2z^2\left(72r^3+144r^2+168r+114\right)\right]\\
&+192\Gamma^{10}(1-r)\left[y^2\left(12r^2+8r+8\right)+z^2\left(3r^2-2r+7\right)-12yz(1+r)\right]\\
&+1920\Gamma^{12}(1-r)+\mathcal{O}(\Delta)
\end{aligned}
\tag{120}
$$

$$
\begin{aligned}
D^5\left[A_0^{(5)}-20\tau A_0^{(3)}\right] &= -\frac{1}{8}y^5r\left(1-r^2\right)\left(1+r^2\right)(z-y)^{10}\\
&-\frac{5}{8}\Gamma^2\left(1-r^2\right)(z-y)^8\left[z^2(1+r)^2+y^2\left(8r^3+r^2+10r+1\right)+yz\left(-4r^3-2r^2-8r-2\right)\right]\\
&-\frac{5}{4}\Gamma^4y\left(1-r^2\right)(z-y)^6\left[3z^4+y^4\left(64r^3+12r^2+88r+15\right)+z^3y\left(-6r^2-12r-18\right)\right.\\
&\qquad\left.+y^3z\left(-64r^3-30r^2-124r-42\right)+y^2z^2\left(16r^3+24r^2+64r+42\right)\right]\\
&+5\Gamma^6\left(1-r^2\right)(z-y)^4\left[3z^5+y^5\left(-128r^3-30r^2-196r-44\right)+y^4z\left(192r^3+84r^2+384r+135\right)\right.\\
&\qquad+z^4y\left(-6r^2-12r-24\right)+z^3y^2\left(16r^3+36r^2+96r+86\right)\\
&\qquad\left.+y^3z^2\left(-96r^3-84r^2-288r-156\right)\right]\\
&+40\Gamma^8(1-r)(z-y)^2\left[y^5\left(-64r^4-90r^3-146r^2-153r-37\right)+z^5\left(r^3+3r^2+3r+5\right)\right.\\
&\qquad+y^4z\left(128r^4+201r^3+367r^2+399r+125\right)+z^4y\left(-4r^4-12r^3-36r^2-47r-39\right)\\
&\qquad+z^3y^2\left(32r^4+66r^3+162r^2+202r+114\right)\\
&\qquad\left.+y^3z^2\left(-96r^4-170r^3-354r^2-408r-168\right)\right]\\
&+32\Gamma^{10}(1-r)\left[y^5\left(-128r^4-308r^3-508r^2-558r-194\right)+z^5\left(4r^4+4r^3+24r^2+59r-1\right)\right.\\
&\qquad+z^4y\left(-40r^4-85r^3-195r^2-485r-155\right)+y^4z\left(320r^4+860r^3+1420r^2+1755r+695\right)\\
&\qquad\left.+z^3y^2\left(160r^4+430r^3+750r^2+1460r+620\right)+y^3z^2\left(-320r^4-905r^3-1495r^2-2235r-965\right)\right]\\
&+960\Gamma^{12}(1-r)\left[z^3\left(2r^3-2r^2+14r-6\right)+y^3\left(-16r^3-16r^2-37r-13\right)\right.\\
&\qquad\left.+z^2y\left(-12r^3+4r^2-57r-1\right)+y^2z\left(24r^3+8r^2+74r+18\right)\right]\\
&+3840\Gamma^{14}(1-r)\left[y(-10r-2)+z(5r-3)\right]+\mathcal{O}(\Delta)
\end{aligned}
\tag{121}
$$

Using the QCD values of the moments to solve (116–120) for the resonance parameters again yields a single, stable, physical solution over the QCD parameter space: $m=(1.38\pm0.13)\,\mathrm{GeV}$, $M=(1.06\pm0.21)\,\mathrm{GeV}$, $\Gamma_{BW}=(0.69\pm0.07)\,\mathrm{GeV}$, $r_m=0.44\pm0.04$, $r_M=1-r_m$. Excellent agreement between the theoretical and phenomenological sides of the normalized Gaussian sum-rules is illustrated by the plots shown in Figure 5.

The value of the fifth-order moment (121) for the resonance parameters corresponding to the central QCD parameters is $A_0^{(5)}-20\tau A_0^{(3)}=-0.192\,\mathrm{GeV}^{10}$, a result which has only a 21% deviation from the QCD value $A_0^{(5)}-$

Resonance Model	$m\,(\mathrm{GeV})$	$M\,(\mathrm{GeV})$	Width (GeV)	$r = r_m - r_M$
Double Narrow	1.41	1.00	0	0.42
Narrow plus Square	1.34	1.24	0.93	0.18
Narrow plus Gaussian	1.38	1.23	0.51	−0.10
Narrow plus Skewed Gaussian	1.40	1.00	0.68	−0.16

Table 2: Resonance parameters obtained from central values of the QCD parameters in the various two-resonance scenarios. The mass M denotes the state associated with the quoted width. The width parameter quoted for the Gaussian models is the equivalent Breit-Wigner width.

	$S_0 - 12\tau^2 - 12\tau\left(\sigma_0^2 - 2\tau\right)$ (GeV^8)	$A_0^{(5)} - 20\tau A_0^{(3)}$ (GeV^{10})
QCD	0.1698	−0.2433
Double Narrow	0.0737	−0.0502
Narrow plus Square	—	−0.1144
Narrow plus Gaussian	—	−0.1300
Narrow plus Skewed Gaussian	—	−0.1918

Table 3: Comparison of the next-highest moment combinations in the two-resonance scenarios with the QCD values. All values are obtained from the central values of the QCD parameters.

$20\tau A_0^{(3)} = -0.243\,\mathrm{GeV}^{10}$. The skewed Gaussian model is thus in reasonable agreement with the QCD value of the fifth-order residual moment combination.

4 Results and Discussion

The resonance parameters devolving from the central values of the QCD parameters have already been summarized in Table 1 for the single wide resonance models, and Table 2 summarizes the results for the resonance parameters obtained in the double resonance models. We note that in the narrow plus wide resonance scenarios, no assumption was made on which state would be wide, and hence it is interesting that the analysis consistently predicts that the lightest state has the non-zero width. Similarly, Tables 1 and 3 summarize the QCD and predicted values of the moments which serve as a consistency check in each of the models. Based on this criteria, the double resonance models have much better agreement with the QCD prediction than the single wide resonance models. The narrow plus wide resonance model is the most accurate in this respect, with only a 21% deviation from the QCD value of the fifth order asymmetry moment $A_0^{(5)} - 20\tau A_0^{(3)}$.

As illustrated in Figure 4, the single narrow resonance model leads to a significant deviation between the theoretical (QCD) and phenomenological results for the normalized Gaussian sum-rule. The single wide resonance and double resonance models dramatically improve this agreement, and all the models lead to plots which are represented by Figure 5. However, a χ^2 measuring the difference between the theoretical and phenomenological curves over the ranges of $\hat{s}$ and τ used in Figure 5 can be used as another criteria to evaluate the effectiveness of the phenomenological models since it provides a quantitative measure of the difference between the theoretically and phenomenologically determined $k = 0$ Gaussian sum-rules. Table 4 lists this χ^2 at the optimized value $s_0 = 2.3$ GeV^2 in each of the resonance models considered for the central QCD parameters. We see that the double resonance models provide a fit which is an order of magnitude better than any of the non-zero width resonance models. However, the χ^2 is on the order of 10^{-6} for all the double narrow resonance models, and hence does not provide a strong distinction between the various scenarios.

Thus the moment consistency test and χ^2 measure of the agreement between the phenomenological and QCD values of the Gaussian sum-rules clearly favour the double resonance scenarios. However, this χ^2 does not clearly distinguish between the various two-resonance scenarios. Despite this apparent difficulty in distinguishing between the scenarios, the mass of the two states in the various double resonance scenarios are relatively stable, lying in

resonance model	χ^2
unskewed Gaussian	1.21×10^{-5}
unskewed square pulse	1.31×10^{-5}
skewed Gaussian	1.45×10^{-5}
double narrow	1.83×10^{-6}
narrow and square pulse	0.923×10^{-6}
narrow and unskewed Gaussian	0.888×10^{-6}
narrow and skewed Gaussian	0.959×10^{-6}

Table 4: The χ for the fits between the theoretical and phenomenological results for the normalized $k = 0$ Gaussian sum-rules over the ranges of $\hat{s}$ and τ used in Figure 5 for each of the phenomenological models considered. Central values of the QCD parameters have been employed.

the range 1.0–1.4 GeV, with the greatest mass splittings occurring in the double narrow resonance model and in the narrow plus skewed Gaussian resonance model.

5 Conclusions

In this paper, we used QCD Gaussian sum-rules to analyze the scalar glueball sector in an effort to obtain predictions for the hadronic parameters (*i.e.* mass, width, coupling strength) of low-lying scalar glueball states. In our analysis, we incorporated instanton effects and employed a number of phenomenological models more general than the traditional single narrow resonance.

First, we demonstrated that the leading order $k = -1$ Gaussian sum-rule (the only sum-rule which receives a contribution from the LET) leads to results which are unstable under moderate QCD uncertainties: single resonance mass extractions ranged anywhere from 1.0 GeV to 1.8 GeV. This variation is too large to yield a definitive prediction for the mass of the lightest scalar glueball, but does, however, indicate a lower bound of roughly 1 GeV on gluonium mass scales. This observation supports similar results obtained previously in [5, 6] where it was shown that instanton effects serve to increase the scale of masses extracted from the $k = -1$ sum-rule whereby reducing the discrepancy between masses predicted using this $k = -1$ sum-rule and those extracted from $k \geq 0$ sum-rules.

Due to the instability of the $k = -1$ Gaussian sum-rule analysis, we turned to the $k = 0$ sum-rule. We showed that hadronic parameters extracted using a single narrow resonance model led to poor agreement between theory and phenomenology as indicated by the plots of Figures 3 and 4. Consequently, we then considered phenomenological models which allowed for resonance strength to be distributed over an appreciable energy range.

We focused on three single non-zero width resonance models (see Section 3), and the results of all the corresponding analyses were indicative of a ($m \approx 1.2$–1.3 GeV), wide ($\Gamma \approx 0.4$–0.6 GeV) resonance (see Table 1). The coincidence between plots of the theoretical and phenomenological Gaussian sum-rules (characterized by Figure 5) represented a vast improvement over the corresponding graphs obtained from a single narrow resonance analysis (Figure 4). However, as indicated in Table 1, all three models failed completely to predict the value of the first independent moment combination $A_0^{(3)}$, prompting us to move on to analyses of phenomenological models that allow for a second resonance.

Regarding both a χ^2 measure of the discrepancy between theoretical and phenomenological $k = 0$ Gaussian sum-rules and the ability to accurately predict higher order, independent moments, the double resonance models represented a marked improvement compared to the single non-zero width resonance models. Resulting hadronic parameter estimates from the various models analyzed are summarized in Table 2. Estimates of the larger of the two masses (m) were remarkably insensitive to the particular width model used, approximately 1.4 GeV in all cases considered. Mass predictions for the lighter of the two resonances (M) ranged from 1.0 GeV in the double narrow and narrow plus skewed Gaussian models to roughly 1.25 GeV in the narrow plus square and narrow plus Gaussian models—again, a surprising degree of stability considering the variety of width models employed. Further, in those models which allowed for a non-zero resonance width, we made no *a priori* assumptions as to which of the two resonances was wide; however, the width was consistently found to be associated with the lighter of the two states and was relatively large in magnitude, yielding an equivalent Breit-Wigner width of $\Gamma_{\rm BW} \approx 0.55\,{\rm GeV}$ in the Gaussian resonance models. These hadronic parameter estimates were subsequently employed in predictions of higher order, independent moment combinations. The results of this analysis are summarized in Table 3. The deviation of the phenomenological predictions from the values computed using QCD was typically 20–50%, with the best agreement occurring in the skewed Gaussian resonance model. While certainly not perfect, this represented a vast improvement over analogous calculations performed in the various single non-zero width resonance models (see Table 1). Finally, in Table 4, we have collected the results of a χ^2 measure of the difference between the theoretical $k = 0$ Gaussian sum-rules and the various phenomenological sum-rules corresponding to each of the resonance models considered. For the double resonance models, the values quoted were consistently an order of magnitude lower than those pertaining to the single non-zero width models. Therefore, in addition to our previous conclusion concerning the necessity for distributed resonance strength, we note further that a single non-zero width resonance model is insufficient to account for this spreading and that far better consistency between theory and phenomenology (as encapsulated in the Gaussian sum-rules of scalar gluonium) is achieved by employing models which allow for a second resonance.

Although certainly relevant to the nature of the spectrum of scalar states with masses under 2 GeV, it is difficult to make a direct comparison between our results and the entries of the PDG [11] since the typical mass separation between the various observed scalar states is relatively small: on the order of 0.2 GeV. Unfortunately, this is approximately the same magnitude as the uncertainties we calculate in our mass estimates. These error bars are the direct result of uncertainties in the QCD parameters (52,56). Therefore, in light of these uncertainties, we refrain from drawing definitive conclusions concerning the nature of any specific scalar state. Instead, we merely note that certain classification schemes proposed by Minkowski and Ochs [27] and Narison [4] require a relatively light (≈ 1 GeV), wide state—a situation completely consistent with our results. Furthermore, the persistent $m = 1.4$ state we find may indeed have ramifications regarding the nature of either the $f_0(1370)$ or the $f_0(1500)$ [28].

Acknowledgements: The authors are grateful for research support from the Natural Sciences and Engineering Research Council of Canada (NSERC).

References

[1] V.A. Novikov, M.A. Shifman, A.I. Vainshtein and V.I. Zakharov, Nucl. Phys. B165 (1980) 67.

[2] M.A. Shifman, Z. Phys. C9 (1981) 347;
P. Pascual and R. Tarrach, Phys. Lett. B113 (1982) 495;
S. Narison, Z. Phys. C26 (1984) 209;
C.A. Dominguez and N. Paver, Z. Phys. C31 (1986) 591;
J. Bordes, V. Gimènez and J.A. Peñarrocha, Phys. Lett. B223 (1989) 251;
J.L. Liu and D. Liu, J. Phys. G19 (1993) 373;
L.S. Kisslinger, J. Gardner and C. Vanderstraeten, Phys. Lett. B410 (1997) 1;
Tao Huang, Hong Ying Jin and Ai-lin Zhang, Phys. Rev. D59 (1998) 034026.

[3] S. Narison and G. Veneziano, Int. J. Mod. Phys. A11 (1989) 2751;
E. Bagan and T.G. Steele, Phys. Lett. B243 (1990) 413.

[4] S. Narison, Nucl. Phys. B509 (1998) 312.

[5] E.V. Shuryak, Nucl. Phys. B203 (1982) 116;
Hilmar Forkel, hep-ph/0005004;
Hilmar Forkel, hep-ph/0103204.

[6] D. Harnett, T.G. Steele and V. Elias, Nucl. Phys. A686 (393) 2001.

[7] A. Belavin, A. Polyakov, A. Schwartz and Y. Tyupkin, Phys. Lett. B59 (1975) 85;
G. 't Hooft, Phys. Rev. D14 (1976) 3432;
C.G. Callan, R. Dashen and D. Gross, Phys. Rev. D17 (1978) 2717;
M.A. Shifman, A.I. Vainshtein and V.I. Zakharov, Nucl. Phys. B165 (1980) 45.

[8] R.A. Bertlmann, G. Launer and E. de Rafael, Nucl. Phys. B250 (1985) 61.

[9] G. Orlandini, T.G. Steele and D. Harnett, Nucl. Phys. A686 (261) 2001.

[10] V.A. Novikov, M.A. Shifman, A.I. Vainshtein and V.I. Zakharov, Nucl. Phys. B191 (1981) 301.

[11] D.E. Groom *et al*, Eur. Phys. J. C15 (2000) 1.

[12] K.G. Chetyrkin, B.A. Kneihl and M. Steinhauser, Phys. Rev. Lett. 79 (353) 1997.

[13] E. Bagan and T.G. Steele, Phys. Lett. B234 (1990) 135.

[14] T. Schäefer and E.V. Shuryak, Phys. Rev. Lett. 75 (1995) 1707.

[15] B.V. Geshkenbein and B.L. Ioffe, Nucl. Phys. B166 (1980) 340;
B.L. Ioffe and A.V. Samsonov, Phys. of Atom. Nucl. 63 (2000) 1527.

[16] M. Abramowitz and I.E. Stegun, *Mathematical Functions with Formulas, Graphs, and Mathematical Tables* (National Bureau of Standards Applied Mathematics Series, Washington) 1972.

[17] S. Narison and E. de Rafael, Phys. Lett. B103 (1981) 57.

[18] T.G. Steele and V. Elias, Mod. Phys. Lett. A13 (1998) 3151.

[19] K.G. Chetyrkin, B.A. Kneihl and M. Steinhauser, Nucl. Phys. B510 (1998) 61.

[20] R. Shankar, Phys. Rev. D15 (1977) 755;
R.G. Moorhouse, M.R. Pennington, G.G. Ross, Nucl. Phys. B214 (1977) 285;
K.G. Chetyrkin, N.V. Krasnikov, N.N. Tavkhelidze Phys. Lett. 76B (1978) 83;
E.G. Floratos, S. Narison, E. de Rafael, Nucl. Phys. B155 (1979) 115.

[21] S. Narison, Nucl. Phys. B (Proc. Supp.) 54A (1997) 238.

[22] M.A. Shifman, A.I. Vainshtein and V.I. Zakharov, Nucl. Phys. B147 (1979) 385,448;
L.J. Reinders, H. Rubenstein and S. Yazaki, Phys. Rep. 1 (1985) 1.

[23] E. Bagan, J.I. Latorre, P.Pascual and T. Tarrach, Nucl. Phys. B254 (1985) 555.

[24] E.V. Shuryak, Nucl. Phys. B203 (1982) 93.

[25] V. Elias, A.H. Fariborz, M.A. Samuel, Fang Shi, T.G. Steele, Phys. Lett. B412 (1997) 131;
V. Elias, A.H. Fariborz, Fang Shi, T.G. Steele, Nucl. Phys. A633 (1998) 279.

[26] V.A. Novikov, M.A. Shifman, Z. Phys. C8 (1981) 43;
M.A. Shifman, Z. Phys. C9 (1981) 347.

[27] P. Minkowski and W. Ochs, Eur. Phys. J C9 (1999) 283.

[28] C. Amsler and F.E. Close, Phys. Rev. D53 (1996) 295;
L. Burakovsky and P.R. Page, Phys. Rev. D59 (1999) 014022.

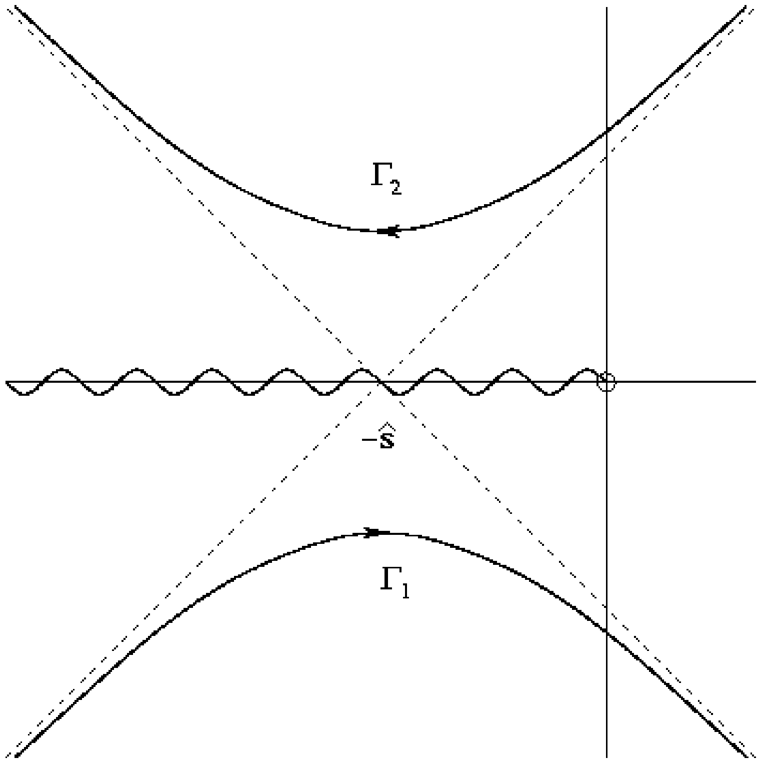

Figure 1: Contour of integration $\Gamma_1 + \Gamma_2$ defining the Gaussian sum-rule in (25). The wavy line on the negative real axis denotes the branch cut of $\Pi(w)$.

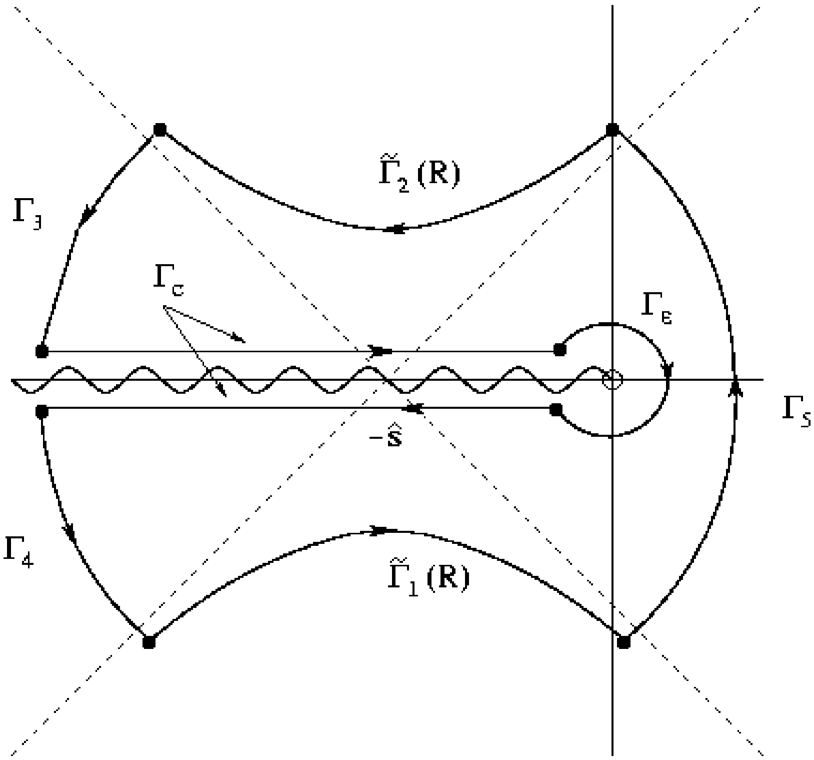

Figure 2: Closed contour $C(R)$ used to calculate the Gaussian sum-rule defined by (25). The inner circular segment Γ_ϵ has a radius of ϵ, and the circular segments Γ_3, Γ_4 and Γ_5 have a radius R. The wavy line on the negative real axis denotes the branch cut of $\Pi(w)$, and the linear segments of the contour above and below the branch cut are denoted by Γ_c. The contour $\tilde{\Gamma}_1(R)$ is that portion of Γ_1 (see Figure 1) which lies in the interior of a circle of radius R centered at $-\hat{s}$, and similarly for $\tilde{\Gamma}_2(R)$.

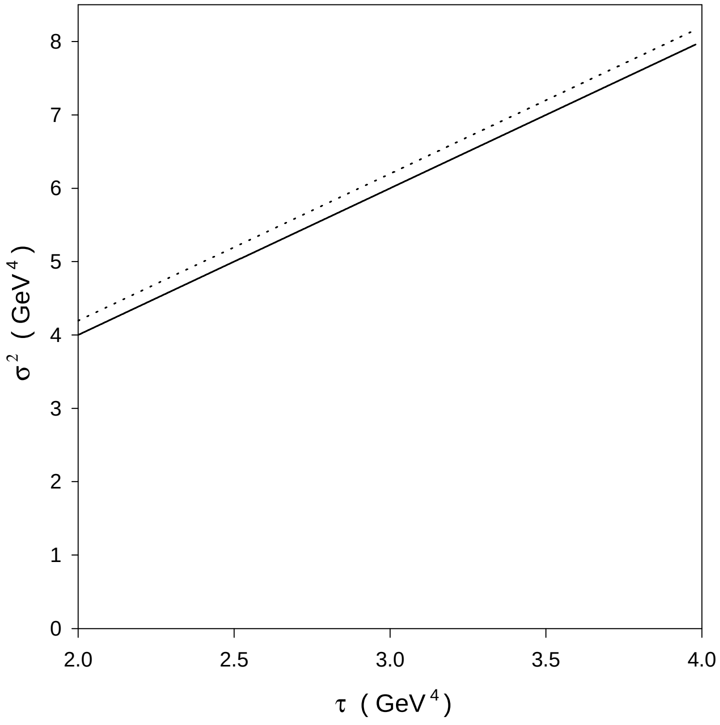

Figure 3: Plot of σ_0^2 for the theoretical prediction (dotted curve) compared with $\sigma_0^2 = 2\tau$ for the single-resonance model (solid curve) for the $k = 0$ sum-rule using the χ^2-optimized value of the continuum $s_0 = 2.3\,\mathrm{GeV}^2$.

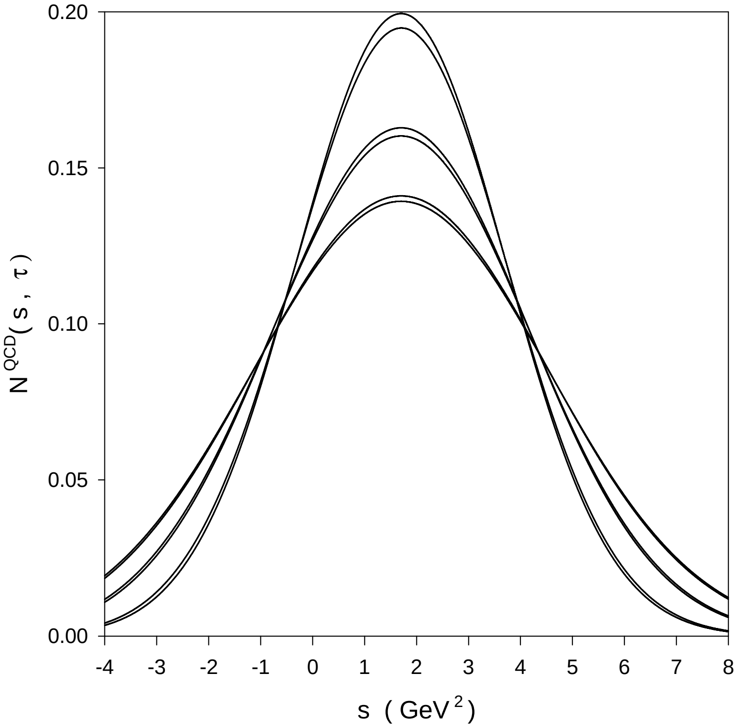

Figure 4: Comparison of the theoretical prediction for $N_0^{QCD}(\hat{s},\tau,s_0)$ with the single narrow resonance phenomenological model (58) using the χ^2-optimized values of the resonance mass ($m = 1.30\,\mathrm{GeV}$) and continuum ($s_0 = 2.3\,\mathrm{GeV}^2$). The τ values used for the three pairs of curves, from top to bottom in the figure, are respectively $\tau = 2.0\ \mathrm{GeV}^4$, $\tau = 3.0\ \mathrm{GeV}^4$, and $\tau = 4.0\ \mathrm{GeV}^4$. The phenomenological model is consistently *larger* than the theoretical prediction near the peak, but is consistently *smaller* than the theoretical prediction in the tails. Central values of the QCD parameters have been used.

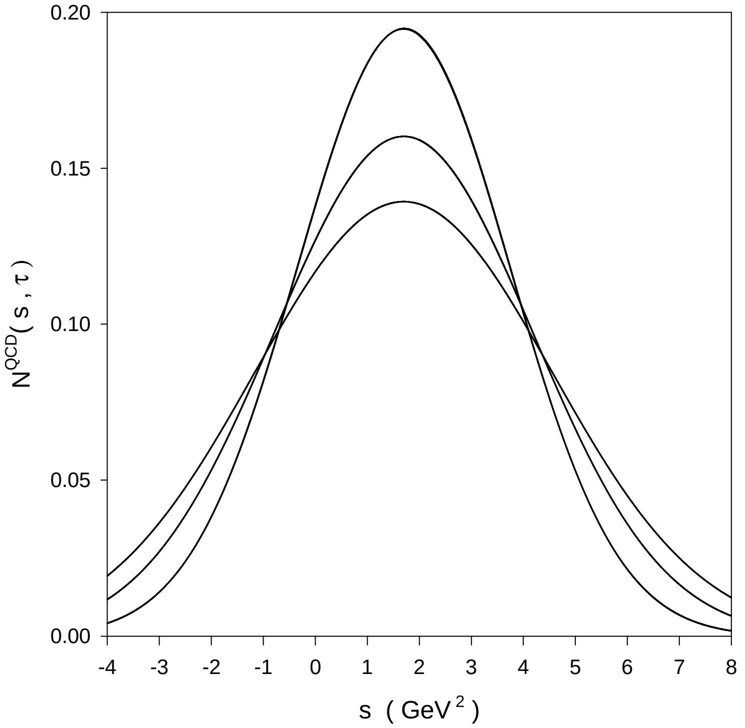

Figure 5: Typical comparison of the theoretical prediction $N_0^{QCD}(\hat{s},\tau,s_0)$ with the phenomenological side of the normalized Gaussian sum-rule (51) in the single non-zero width resonance models and the double resonance models. Individual plots for each model are indistinguishable from those shown, and are hence not repeated as additional Figures. The χ^2-optimized value of the continuum ($s_0 = 2.3\,\mathrm{GeV}^2$) has been used to extract the resonance parameters as outlined in the text. The τ values used for the three pairs of curves, from top to bottom in the figure, are respectively $\tau = 2.0$ GeV^4, $\tau = 3.0$ GeV^4, and $\tau = 4.0$ GeV^4. Note the almost perfect overlap between the theoretical prediction and the phenomenological models. Central values of the QCD parameters have been used.